EARTH SCIENCES
RESEARCH JOURNAL
Earth Sci. Res. J. Vol. 29, No. 2 (June, 2025):167 - 181

UNIVERSIDAD NACIONAL DE COLOMBIA

GEOLOGY

Geochemical data from the Tanuma carbonate reservoir (Central Iraq) indicate higher terrigenous input and deoxygenation during the Coniacian- Early Santonian age

Rana Abbas Ali [1],*

1 Department of Geology, College of Science, University of Baghdad, Iraq

*Corresponding author E-mail: rana.ali@sc.uobaghdad.edu.iq

ABSTRACT

Oceanic anoxic events were characterized by the widespread deposition and accumulations of pelagic sediments rich in organic matter, such as black shales, and are considered key mechanisms for organic carbon burial and, in such, buffering Cretaceous runaway super-greenhouse. A negative carbon isotopic excursion (CIE), typically overlaid atop a long- term positive pattern, and significant environmental and climatic shifts are two characteristics that identify the Coniacian–Santonian, according to a variety of sedimentary records. But there is still no evidence to support the theory that variations in oceanic deoxygenation and continental weathering input in shallow seas could contribute to the carbonate-platform crisis at low latitudes. Here, carbonate content and carbonate-hosted elements from the Tanuma carbonate platform in Central Iraq (East Baghdad Oilfield; EB10 well) are analyzed for the Coniacian–Early Santonian transitional phase. The OAE3 boundary is marked by a clear increase in the elements that are most water insoluble (such as Al, Sc, Th, Ti, and all of the rare earth elements), followed by a slight increase or relatively high levels throughout the OAE CIE's negative phase. These results suggest that the increased terrigenous input was likely linked to rapid global warming during the Coniacian–Santonian period, contributing to widespread carbonate platform degradation. The increase in the abundance of these water-insoluble elements is immediately followed by an increase in the Mn, Ce, and Ce anomaly, which are then better values throughout the negative CIE interval. These findings align with similar deoxygenation trends observed in contemporaneous carbonate platforms across Egypt and the southern Tethys, indicating a potentially widespread oceanic anoxic event during the Coniacian–Santonian interval. These events were probably related to increased nutrient input and continental weathering, which favoured oxygen consumption as well as primary productivity. In CIE's recovery phase, the stratigraphically elevated insoluble in water elements exhibit a gradually declining trend in parallel to heightened redox proxy values, indicating a drop in the intensity of continental weathering and associated second deoxygenation at shallow seas. In this case, increased recycling in bioessential nutrients or a slowing of the ocean's circulation could have contributed to deoxygenation. The interdependent connection among carbonate content, geochemical data, and biotic changes indicates that 1- The Tanuma carbonate platform probably noticed a minor degradation around the OAE3 boundary period due to the beginning of increasing terrigenous input and the deoxygenation of shallow seas. 2- During the CIE's negative phase, the heightened terrigenous input and deoxygenation probably contributed significantly to the more serious situation facing benthic carbonate producers.

Keywords: Coniacian–Santonian OAE3, major and trace elements, carbonate platform, shallow coastal facies, Central Iraq

Los datos geoquímicos del yacimiento carbonatado de Tanuma (Irak central) indican un mayor aporte terrígeno y desoxigenación durante la era Coniaciense-Santoniano temprano

RESUMEN

Los eventos anóxicos oceánicos se caracterization por extensas deposiciones y acumulaciones de sedimentos pelágicos ricos en materia orgánica, tales como shales negros, y son considerados mecanismos claves para el enterramiento de carbón orgánico y, en estos casos, almacenamiento del superinvernadero del Cretácico. Una excursión negativa isotópica del carbono (CIE, del inglés carbon isotopic excursion, típicamente sobrepuesta sobre un patrón positivo de largo período, junto con los cambios significativos climáticos y ambientales son características que identifican el período entre el Coniaciano y el Santoniano, de acuerdo con una amplia variedad de registros sedimentarios. Pero no hay evidencia que fundamente la teoría de que las variaciones en la desoxigenación y la meteorización continental en aguas marítimas someras pudieron contribuir a la crisis de las plataformas carbonatadas en las bajas latitudes. En este estudio se analiza el contenido de carbonato y los elementos alojados en carbonato de la plataforma de Tanuma, en el centro de Irak (campo petrolífero de Bagdad Oriental; pozo EB10), para la fase de transición Coniaciense-Santoniano temprano. El límite OAE3 está marcado por un claro aumento en los elementos que son más insolubles en agua (como Al, Sc, Th, Ti y todos los elementos de tierras raras), seguido de un ligero aumento o niveles relativamente altos a lo largo de la fase negativa del CIE OAE. Estos resultados sugieren que el aumento de la entrada terrígena probablemente estuvo relacionado con el rápido calentamiento global durante el período Coniaciense-Santoniano, lo que contribuyó a la degradación generalizada de la plataforma carbonatada. El aumento en la abundancia de estos elementos insolubles en agua es seguido inmediatamente por un aumento de Mn, Ce y Ce anómalo, que luego son mejores valores a lo largo del intervalo CIE negativo. Estos hallazgos se alinean con tendencias de desoxigenación similares observadas en plataformas carbonatadas contemporáneas en todo Egipto y el sur de Tetis, lo que indica un evento anóxico oceánico potencialmente generalizado durante el intervalo Coniaciense-Santoniano. Estos eventos probablemente estuvieron relacionados con el aumento de la entrada de nutrientes y la meteorización continental, que favorecieron el consumo de oxígeno, así como la productividad primaria. En la fase de recuperación del CIE, los elementos insolubles en agua estratigráficamente elevados exhiben una tendencia gradualmente decreciente en paralelo al aumento de los valores proxy redox, lo que indica una caída en la intensidad de la meteorización continental y la segunda desoxigenación asociada en mares poco profundos. En este caso, el aumento del reciclaje en nutrientes bioesenciales o una desaceleración de la circulación oceánica podrían haber contribuido a la desoxigenación. La conexión interdependiente entre el contenido de carbonato, los datos geoquímicos y los cambios bióticos indican que, 1. La plataforma carbonatada de Tanuma probablemente notó una degradación menor alrededor del período límite OAE3 debido al comienzo del aumento de la entrada terrígena y la desoxigenación de mares poco profundos. 2- Durante la fase negativa del CIE, la mayor entrada terrígena y la desoxigenación probablemente contribuyeron significativamente a la situación más grave que enfrentan los productores de carbonato bentónico.

Palabras clave: Coniaciense-Santoniano; OAE3; elementos mayores y elementos traza; plataforma carbonatada; facies someras costeras; Central Iraq.

Record
Manuscript received: 19/10/2024
Accepted for publication: 14/05/2025

How to cite this item:
Ali, R. A. (2025). Geochemical data from the Tanuma carbonate reservoir (Central Iraq) indicates higher terrigenous input and deoxygenation during Coniacian-Early Santonian age. *Earth Sciences Research Journal, 29*(2), 167-181. https://doi.org/10.15446/esrj.v29n2.117124

ISSN 1794-6190 e-ISSN 2339-3459
https://doi.org/10.15446/esrj.v29n2.117124

1. Introduction

The Coniacian-Early Santonian Period (~ 88.5-86.5 Ma) experienced one of the most well-known Oceanic Anoxic Events (OAEs) due to the broadening of oxygen-depleted oceans and the global dispersion of coeval organic-rich sediment originating from epicontinental and pelagic settings (Jenkyns, 2003, 2010). This geological time interval was marked by major climatic and ecological perturbations, such as peak warming of the world's oceans in the late Cenomanian to Santonian (Jenkyns, 1980; Schlanger & Jenkyns, 1976; Hu et al., 2012; Kaya et al., 2020; Mansour & Wagreich, 2022), improved continental weathering (Brazier et al., 2015; Chenot et al., 2018; Petrizzo et al., 2022), substantial rise in sea levels (Haq, 2014; Chen et al., 2015; Yilmaz et al., 2018; Mansour et al., 2020a), acidification of the oceans (Dameron et al., 2017; Steuber et al., 2023), and biological crisis (Keller, 2008; Labandeira et al., 2016). These complicated paleoenvironmental and climatic events were linked to large geological perturbations in the Earth system, specifically the Earth's carbon cycle (Schlanger & Jenkyns, 1976; Jenkyns, 2010; Wagreich, 2012). These complicated geological phenomena are distinguished by global deposits of organic shales linked to significant carbon isotope excursions (CIEs) (Leckie et al., 2002; Tsikos et al., 2004).

Improved continental silicate weathering directly consumes inorganic carbon during OAEs, increasing nutrient supply to the oceans. As a result, oxygen-depleted waters expand, enhancing marine organic matter productivity and its resulting burial in the ocean: a phenomenon that may have been crucial in lowering excess CO_2 in the atmosphere (Schlanger & Jenkyns, 1976; Jenkyns, 2010, as well as references therein). Despite the fact that these two environmental shifts were widely identified by numerous systems of isotope (e.g., osmium, strontium, molybdenum, calcium, thallium, nitrogen, and sulphur) throughout the OAE (e.g., Peucker-Ehrenbrink & Ravizza, 2000; Jones, 2001; Wendler et al., 2009; Blättler et al., 2011; Chamberlain et al., 2013; Cao et al., 2016; Sun et al., 2016; Cao et al., 2021), sections from the southern and northern hemispheres make up the vast majority of the research, primarily from the Atlantic Ocean and neighbouring basins, Africa, and Central Asia. Despite several studies focusing on $\delta^{34}S$ measurements in Asian carbonate-associated sulphates, high-resolution geochemical assessments from the Mesopotamian Basin remain scarce, warranting this investigation (Cao et al., 2016; Cao et al., 2021). The sulphur-isotope measurements, however, have been seen as a potentially changed signal due to the substantially bigger magnitude $\delta^{34}S$ values in comparison to those in coeval Asian sediments (Xu et al., 2023). Nederbragt et al. (2004) propose a positive cycle of feedback between oxygen depletion, phosphate regenerating and oceanic production during the OAEs. OAEs may have been caused or accompanied by enormous injections of clathrate-trapped methane into the atmosphere (Jenkyns, 2003). Carbonate platforms of shallow water were particularly common in the tropical and subtropical regions along the borders of southern Tethys throughout the Coniacian-Early Santonian, where shallow-water systems rich in biological diversity were found (Jarvis et al., 2002; Phelps et al., 2015; Yilmaz et al., 2018; Smith et al., 2021; Mansour & Wagreich, 2022). Those biotic carbonate platforms had been generally modified by a diversity of planktonic foraminifers, calcispheres, calcareous nannofossils, and corals tracing the evolution of Cretaceous sea levels, while a diversity of larger benthic foraminifers, dasycladalean algae, corals, and rudist bivalves reveal substantial decreases at the time of oceanic anoxic events (OAEs) (Jarvis et al., 2002; Pohl et al., 2020; Steuber et al., 2023). The ultimate reaction of these shallow-marine systems to significant worldwide palaeoceanographic and palaeoenvironmental disruption resulted in the Tethyan carbonate platforms' foundering and drowning. Benthic ecosystems and the formation of shallow-water carbonate in the past geologically are generally considered to be negatively impacted by enhanced terrigenous inputs and oxygen depletion (Blättler et al., 2011; Korbar et al., 2012; Clarkson et al., 2018; Han et al., 2022). However, reliable chemical proxies of carbonate platforms for shallow water, which can accurately record information on global and/or regional shifts in terrigenous intake and supply of oxygen, are scarce (Han et al., 2022; Mansour & Wagreich, 2022). Pulses of terrigenous input had been identified in the Coniacian-Early Santonian of Morocco's High Atlas Platforms, which may have been a crucial controlling element in the closure of this carbonate factory (Sachse et al., 2012; Andrieu et al., 2022; Algouti et al., 2023). There have been investigations into redox conditions using carbonate-hosted I/Ca, Mn/Ca, and Ce anomalies (Ce/Ce*) on the Campania-Lucania Platform, Italy, as well as TOC, S, Al, and $CaCO_3$ from the Demerara Rise (NW South American edge) (März et al., 2009; Lu et al., 2010), and the bulk-rock hosted Al, Si, Fe, Ti, P, Cr, Sr, Ba, Zr, V, Ni, Zn, Co, and Mo in the southern Tethys (Egypt) (Mansour et al., 2020b). These redox proxies indicate a decrease in oxygen content in shallow tropical waters, but this is inconsistent with sedimentological evidence of limestones with high bioturbation density in the Niobrara Formation of the Western Interior Seaway and reddish oxygenated claystone in southern Tibet during the OAE3 interval (Wagreich, 2009; Lowery et al., 2017). As a result, the precise role of accelerated continental weathering and anoxia in promoting a neritic carbonate crisis is still debated. The Cretaceous had a number of global oceanic anoxic episodes (OAE), which are characterized by the extensive accumulation of stratified organic-rich sediments. The paleogeographic distribution of organic-rich sediments suggests that the Coniacian-Santonian OAE (= OAE3) was more reliant on local or regional conditions than it was on a global scale. Within the equatorial basins, these are primarily found in shallow water environments and epicontinental seas (Bomou et al., 2013). Therefore, it is necessary to focus on studying several sections from different paleogeographic regions and at different paleodepths in central Iraq in order to identify oceanic anoxic events for hydrocarbon exploration.

The shallow-water Tanuma Carbonate Platform's East Baghdad 10 (EB10) well has been well investigated for biostratigraphy, sedimentology, and hydrocarbon characterization in the Northern Hemisphere, allowing confirmation of the typical OAE (Aqrawi, 1996; Ali et al., 2022; Ali, 2023a, b). The major and trace elements and $CaCO_3$ content of shallow-marine carbonate of the Coniacian-Santonian transitioning phase of the EB10 well are presented here with the aim to estimate variations in continental weathering along with ocean deoxygenation at shallow tropical waters within the Northern Hemisphere's southern Tethys. The results from this investigation are later combined with data from the Tethys Ocean's western margin, the African shelf, and Southern Tibet to determine the degree of global shifts potentially influencing carbonate platforms throughout this time span at the supra-regional Tethyan scales.

2. Geological setting and stratigraphy

The study area is in the East Baghdad Oilfield in the Mesopotamian Foredeep Basin, which is a large section of the Zargos Fold Belt (Figs. 1 and 2). As the region experienced a relative decline in sea level, the first precursors of the Tanuma Formation facies began gradual sedimentation, resulting in varying facies that reflected the shallowness and degree of turbulence of the water on the one hand and the nature of the topography of the sedimentary basin that reached that period on the other (Aqrawi, 1996; Al-Ameri, 2011; Ali & Jassim, 2023). The seventh facies range, named the shelf basin and also known as the open platform, represents the base of the Tanuma Formation in the secondary basin area (Baghdad Basin). This basin is distinguished by its fine-grained carbonate sediments that contain organic detritus, which is a lime mudstone facies (Fig. 3a).

The Lower Tanuma Formation facies were deposited in somewhat distinct coastal facies locations, but they all have one thing in common: they are shallow and show an obvious regressive facies pattern (Sadooni, 2004; Abdel-Fattah et al., 2022; Gharib et al., 2024). The relatively unstable climatic and tectonic conditions at the beginning of the Coniacian resulted in somewhat varied, shallow coastal facies zones, although they all share a marked regressive facies pattern (Fayadh et al., 2018; Mahdi et al., 2019). The bottom of the Baghdad Basin began to gradually stabilize. This basin's sediments were created by a geological sequence of black shale and shale limestone. In general, the Tanuma Fm. distinctive sequence is composed of an alternation of bioclastic-bearing lime mudstone facies (Fig.3b) and rotaliid-bearing clastic lime mudstone facies (Fig.3c). These facies indicate the open platform (shore platform) that has been successively exposed to the impact of the open sea, resulting in the emergence of two distinct water movement and circulation systems, namely restricted circulation and open circulation. The features of the secondary basin became prominent near the middle of the Tanuma Fm. sequence, causing a partial marine transgression from the eastern and northeastern sides, covering the entire study area and causing open water circulation and free interaction with the open sea. As a result, the black shale sediments began to disappear, to be replaced by a calcareous succession consisting of a bioclastic lime wacke

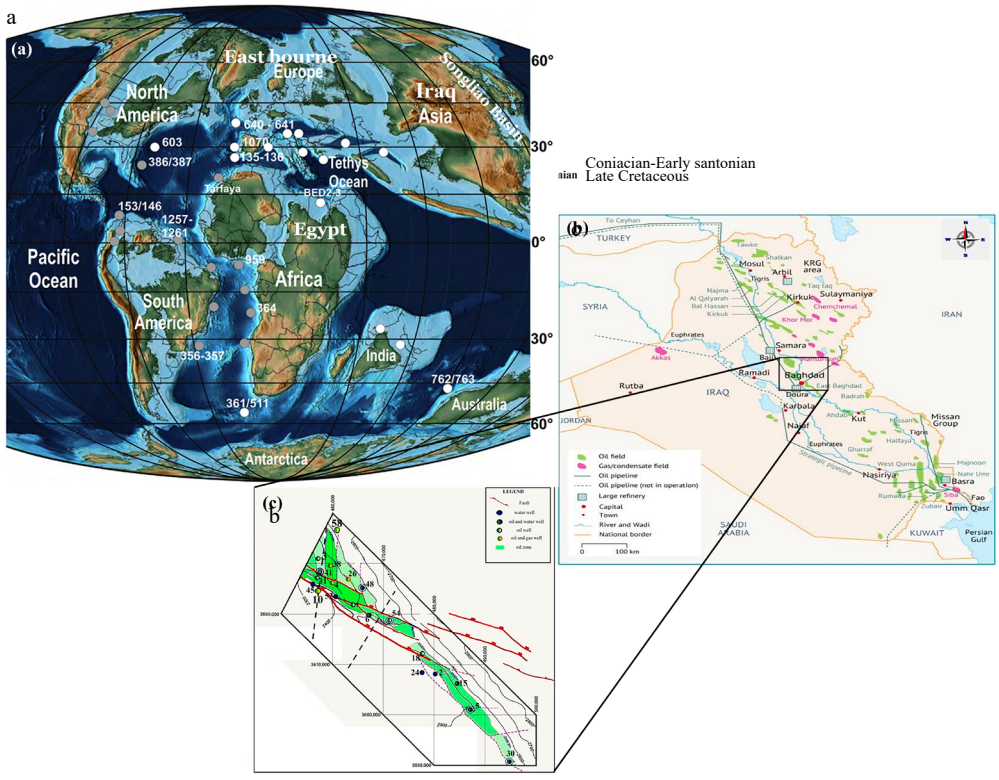

Figure 1. The location of the East Baghdad Oilfield. (a) Location of the studied Coniacian-Santonian OAE in the northeast of Asia (late Cretaceous plate tectonic map for 86 Ma modified from Wagreich (2009, 2012); (b) An Iraqi location map showing the basins and oil fields on the country's northeastern Arabian Peninsula. (c) A map of central Iraq showing the locations of the study's wells.

mudstone facies bearing globigerina and calcospherites (Fig. 3d) and a rotaliid -bearing bioclastic lime wacke mudstone facies (Fig. 3e). These facies reflect varying marine influences, which can be represented by the succession of the third standard facies zone (the edge of the sedimentary basin), where floating organisms breed, and the inner shelf zone, where benthic organisms breed and are influenced by organic detritus rolling from the shallow rims adjacent to it. As a result, it represents a zone of the shelf basin's border and a moderate slope that encompasses the entire research area. Following a series of marine influences, there was an almost abrupt marine transgression from the entire current study area, resulting in two depositional systems parallel to the coastline, one of which is very shallow close to it and has turbulent wave activity, known as the turbulent platform edge, and the other with relatively calm marine conditions. This was reflected in the prevalence of a distinct sedimentary facies known as the coated bioclastic lime wackestone facies (Fig. 3f).

3. Materials and methods

3.1. Sample selection

The Tanuma Fm.'s Coniacian-Early Santonian age samples were recovered from an oil well in the East Baghdad Oilfield (EB10) in Central Iraq (Fig. 2). In particular, numerous storm-generated beds with evident terrigenous composition (e.g., fine-grained quartz and a trace of clay) exist in the bottom portion of the OAE CIE period, potentially contaminating the acetic acid leaching mechanism. Thin sections of these samples were therefore examined first to choose the most well-preserved rock components, which in this study were pure carbonate, free of storm-originating terrigenous grains, and free of indications of metamorphism and recrystallization. Lastly, the samples of Tanuma Fm. are distinguished by grainstones with little wackestone/packestone (Sadooni, 2004). These materials were chopped into newly formed rock chips, which were subsequently micro-drilled to create a powder while being cautious to avoid veins, cement-filled the pores, and bioclasts.

3.2. Calcium carbonate content and elemental concentration

A total of 60 samples were chosen for determination of calcium carbonate content utilizing an NFP18-508 pressure calcimeter. By calculating the partial pressure ratio of the CO_2 produced as a result of the reaction between HCl and $CaCO_3$, this device estimates the $CaCO_3$ contents (wt%). Each bulk sample's carbonate powder was dissolved in excess of 10% HCl, and the volume of CO_2 created was utilized to compute the $CaCO_3$ amount. Every fifteen samples, pure carbonate standards and repeats were used to regulate the variability. This technique's long-term error in instruments is in the range from 0.5% to 3%. We chose 57 bulk carbonate samples obtained from the Tanuma Fm. for element analysis, which generally but not entirely correlate to $CaCO_3$ content samples. Each carbonate sample's powder was weighed and then dissolved in 5 mL of 10% acetic acid. After 12 hours, 0.5 mL of each sample's solution had been transferred to a fresh precleaned Teflon container, then the aliquot was three times dried with 1 mL concentrated HNO_3 to convert the dissolved materials to nitrate. Lastly, these samples had been diluted in 15 mL of 2% HNO_3 solution. At the Iraqi Ministry of Science and Technology's research labs, elemental concentrations were determined using a SHIMADZU PG-990 atomic absorption spectrometer, with a measurement precision of ±5% relative standard deviation (RSD). Internal standards were used to verify elemental concentrations, and the analytical uncertainty after triplication for most elements was +/– 1.5%. Additionally, analyses of the carbonate samples' stable C isotopic compositions were performed. A Finnigan MAT253 mass spectrometer was used to evaluate the substances indicated above. The treatment approach was similar to that reported by Lash (2018). The levels for $\delta^{13}C$ were calculated with δ per unit (‰) in relation to the Viennese-Pee Dee Belemnite (V-PDB) standard and the standards set by the Vienna Standardized Average Oceans Water (V-SMOW). The standard samples utilized were the Chinese standards GBW04415 ($\delta^{13}C$ = +1.51 ± 0.02‰, V-PDB) and GBW04416 ($\delta^{13}C$ = –5.06 ± 0.05‰, V-PDB). The accuracy of those standard specimens' calibration was checked after each three specimens to make sure it was better than 0.2‰.

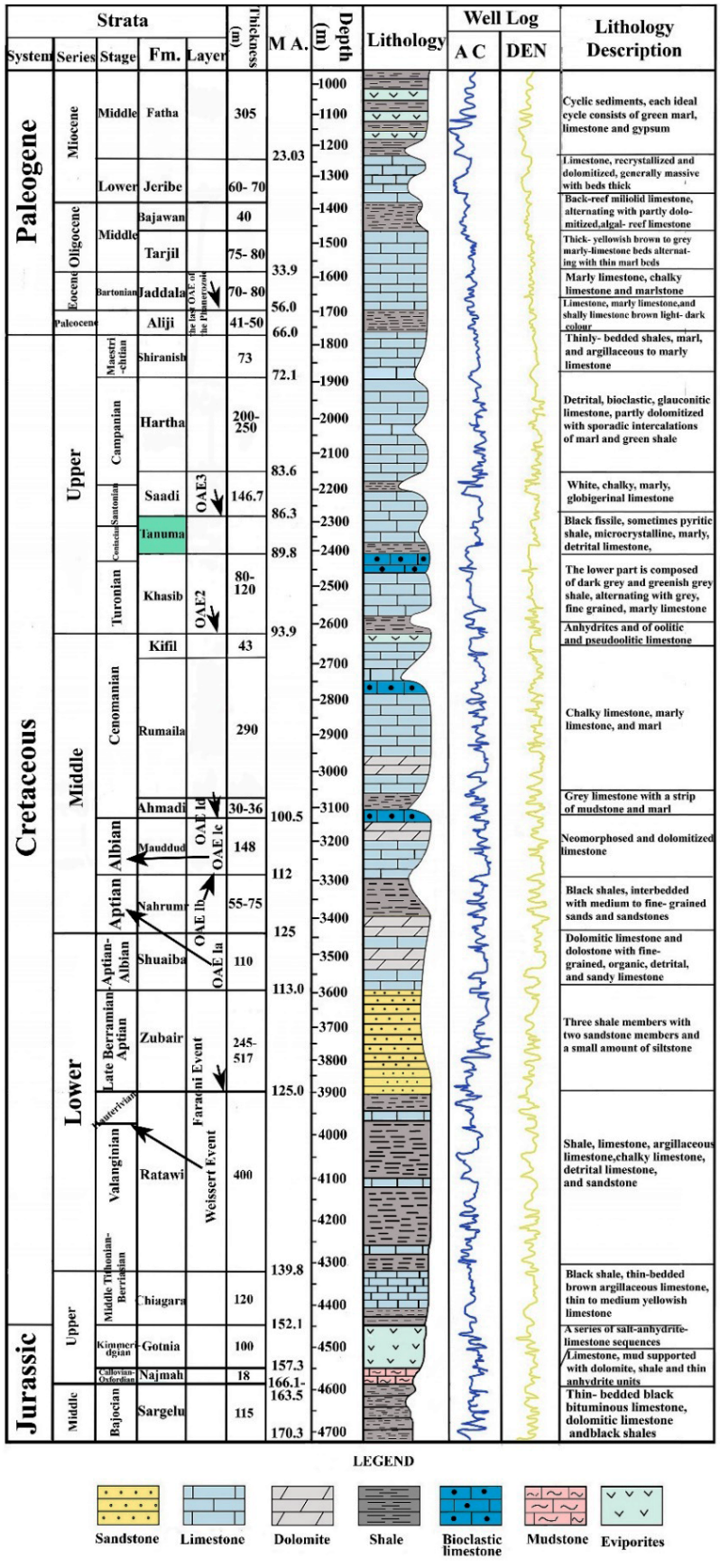

Figure 2. The East Baghdad Oilfield's stratigraphic column.

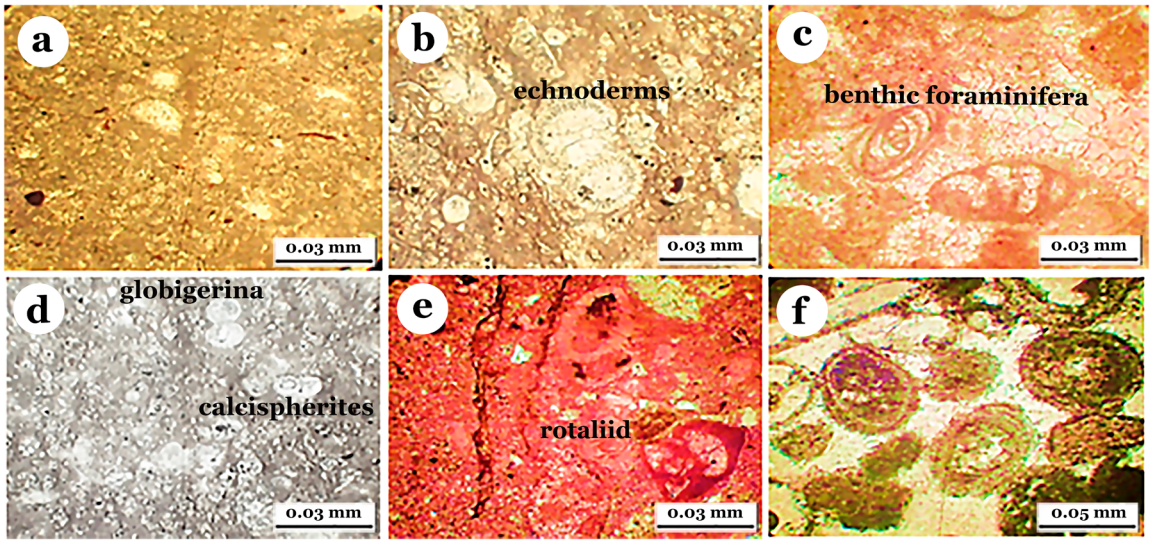

Figure 3. Photomicrographs of Tanuma Fm. depositional facies in the East Baghdad Oilfields of the Mesopotamian Basin. (a): Lime mudstone facies; (b): Bioclastic-bearing lime mudstone facies; (c): Clastic lime mudstone facies; (d): Bioclastic lime wacke mudstone facies bearing globigerina and calcisphere; (e): Rotaliid -bearing bioclastic lime wacke mudstone facies; (f): Coated bioclastic lime wackestone facies.

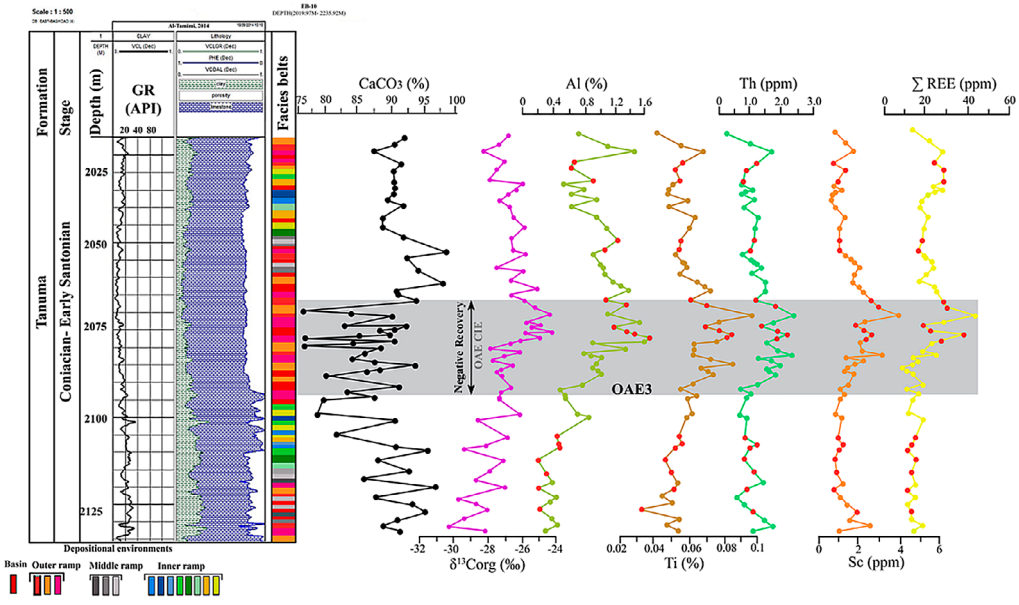

Figure 4. presents geochemical profiles of key water-insoluble elements, $CaCO_3$ concentration, $\delta^{13}C$ org, across the Coniacian–Santonian interval, with color-coded indicators of terrigenous input and deoxygenation events. The hues and red spots of elemental profiles reflect specimens having REE distribution patterns similar to seawater (Fig. 6A) with MREE bulge/hat shaped (Fig. 6B). OAE3: Oceanic Anoxic Event 3.

3.3. The anomalous of Cerium

The relative enrichment or depletion of PAAS is compared to calculate the Cerium anomaly (Ce/Ce*) (Taylor & McLennan, 1985) normalized Ce($[Ce]_{SN}$) to neighbouring non-redox sensitive rare earth elements (REE). Because of the abnormal enrichments of La in seawater, the new recommended computation sans La offered by Lawrence & Kamber (2006) was used in this study: $Ce/Ce^* = [Ce/(Pr \times (Pr/Nd))]_{SN}$.

4. Results

4.1. $CaCO_3$ composition and major element concentrations

The data (given as means ± 1σ standard deviation) reveal that the percentage of $CaCO_3$ ranges from 76.2 to 98.8% (90.03 ± 3.5%, n=60; Fig. 4). The pattern is made up of a steady decline up-section, beginning at the onset

threshold of the OAE CIE at 2093m, extending and culminating throughout the negative period of the OAE CIE, and practically returning to normal levels at the end of the CIE period. The elemental concentrations in Fig. 4 range from 0.2 to 1.7% (0.849 ± 0.1%, n= 60) for Al, 0.04 to 0.094% (0.0596 ± 0.02%, n= 60) for Ti, 0.3 to 2.5 ppm (1.275 ± 0.8 ppm, n= 60) for Th, and 0.2 to 3.9 ppm (1.44 ± 0.09 ppm, n= 60) for Sc. The Sc, Th, and Ti profiles reveal a rapid positive shift at the OAE3 boundary, which is either basically consistent high-level values or a very slight rise (Th and total of REE), but with little fluctuations up to about the CIE threshold's midpoint (Sc and Ti) (Fig. 4). Then, they steadily decrease till the CIE's ultimate level; nevertheless, Al shows a general rise from the OAE3 border to the end of the OAE CIE intervals and maintains comparatively high levels back toward the CIE's end level. Mn values at the EB10 vary from around ~94 to ~219 ppm (144.16 ± 44.5 ppm, n = 60; see Figure 5). A decline from ~160-180 towards ~103 ppm under the OAE3 border is followed by a moderate, slower increase to ~33-40 ppm around the start phase of the OAE CIE, which gets steep, culminating in the CIE's negative phase, which reaches high levels of about 140 ppm. Separating by a decrease in Mn concentration (120-130 ppm), the pattern continued to grow again up the section, peaking near the top level of the OAE CIE at values close to 160 ppm before returning to normal levels just above this level.

4.2. Trace elements concentrations & Ce anomaly (Ce/ Ce)*

Total REE (∑REE) values ranged from 42.0 to 52.08 ppm (48.79 ± 20.4 ppm, n=60). The profile matches that of Ti, Th, and Sc (Fig. 4). The PAAS-normalized pattern demonstrates the fact that REE distribution has been defined in high LREE depletion, relatively HREE enrichment (Fig. 6a), except for a few samples (shown as red spots in the line of Fig. 4), and by an MREE enrichment (hat-shaped pattern; Fig. 6b). Ce values range from 0.54 to 25.8 ppm (7.7 ± 5.3 ppm, n=60), while coupled values of Ce/Ce* range between 0.39 and 1.76 (0.85 ± 0.3, n=60) (Fig. 5). Both the Ce/Ce* ratio and the Ce contents show a generally positive correlation with Mn, except there is an overall positive trend in the Ce/Ce* throughout the period from 1107 to 1122m, and slight variations in Mn and Ce contents.

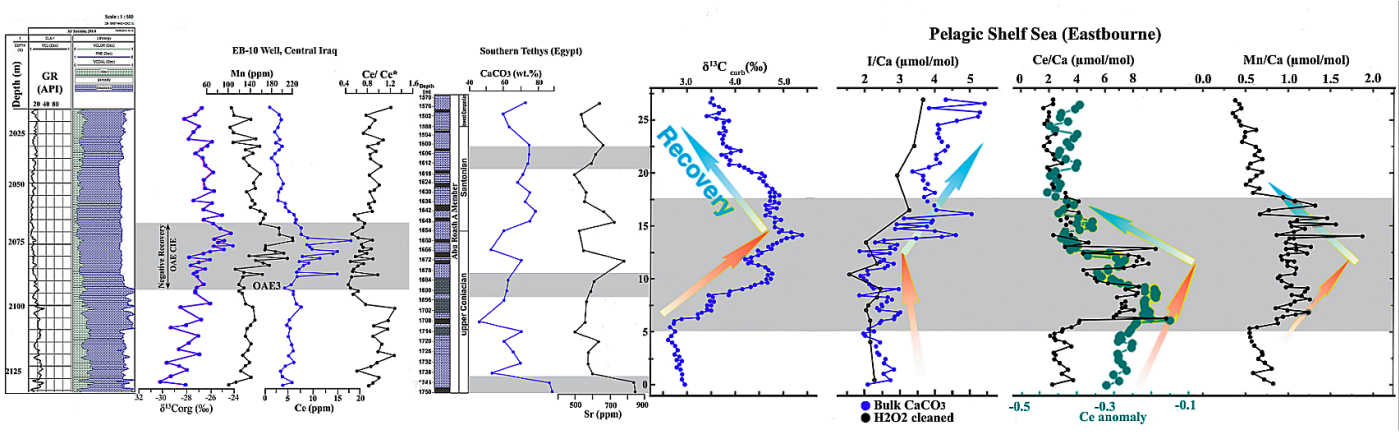

Figure 5. The correlation for geochemical profiles for widely employed redox proxies at Coniacian-Early Santonian carbonates from the southern Tethys (Egypt) and the pelagic shelf sea (Eastbourne). $CaCO_3$ and Sr data for the calcareous sequence of the Abu Roash Formation in the Abu Gharadig Basin (Egypt) are from Mansour et al. (2020b), while $CaCO_3$, $\delta^{13}C$ carb, I/Ca, Ce/Ca, Ce anomaly, and Mn/Ca data for the Late Cretaceous carbonate of the Eastbourne are from Lu et al. (2010).

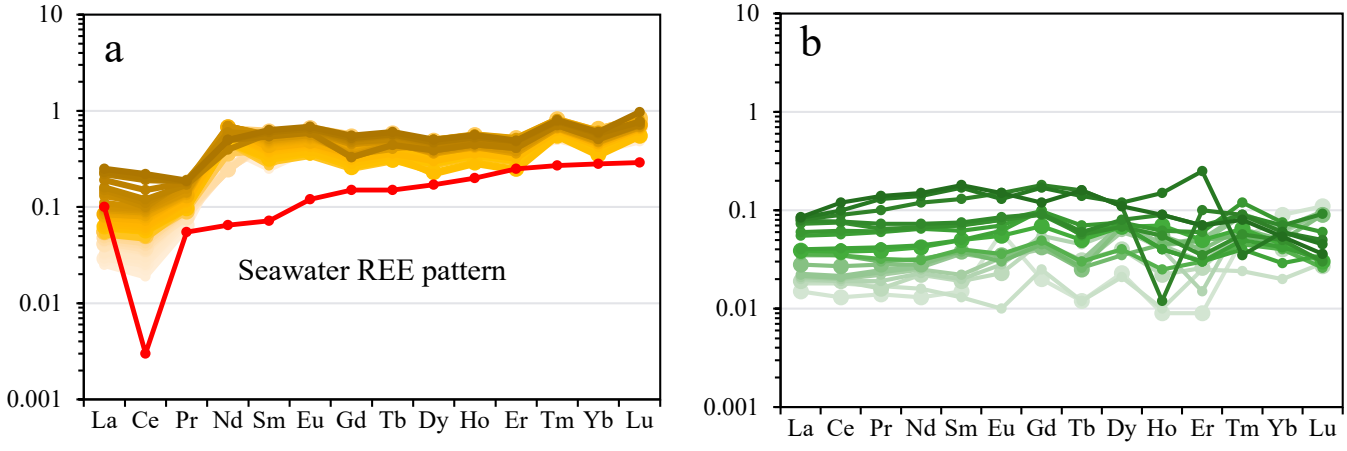

Figure 6. the PAAS-normalized REE distribution pattern for the acetic acid (HAc, 1 N)-leaching liquid of Coniacian-Early Santonian carbonate derived from EB10. a. Seas-like REE structure in the current investigation and present deep Pacific oxia seawater (in red curve), revised by Deng et al., 2017. b. hat-shaped pattern (sample spots highlighted in red in Fig. 4 curve).

5. Discussion

5.1. Elemental clues of terrigenous input & assessment of Ce cycle

Seawater contains a variety of water insoluble elements, including Th, Al, Sc, Ti, and REE, which are primarily caused by rivers' water's chemical weathering and/or the chemical weathering products' dissolution. Terrigenous detritus contains significantly larger amounts of these elements than pure ocean carbonate (Taylor & McLennan, 1985; Su et al., 2017). As a result, the quantities of water-insoluble components of carbonate structures absorbed from peripheral seawater are influenced by terrigenous inflow, giving these compounds a perfect monitoring of continental weathering processes. This analysis eliminated tempestites having coarse siliciclastic components. As indicated in figure 4, the highest water- insoluble Th, Sc, Ti, and REE levels, in addition to Al (excluding the recovered interval for the OAE CIE), are favourably correlated to each other, while negatively linked to the carbonate content, and probably have an overall positive correlation to clay. These data show that such water- insoluble components primarily come from minerals found in clay. Concerning the potential for contamination caused by the leaching technique indicated previously, a threshold level of 1 ppm for Th and 4 ppm for Zr, equating to around 2% siliciclastic contaminants, was established and utilized as a signal of limiting contamination of detrital inputs (Franchi, 2018). The elements measured in this investigation vary between 0.3 to 2.5 ppm (1.27 ± 0.8 ppm) of Th (Fig. 4) and between 0.44 to 7.12 ppm (4.19 ± 2.2 ppm) for Zr, with only 12 and 7 data points, respectively, exceeding the threshold indicated previously. These findings indicate the chemical leaching method probably contaminated just some specimens with siliciclastic particles. Furthermore, the average $CaCO_3$ level is 90.03%, while the six data points with coupled element information are only marginally below 85% (Fig. 4), which is believed to represent a lower threshold for the potential for masking the REE from fractional release of siliciclastic constituents (Cao et al., 2020; Tostevin, 2021). Furthermore, PAAS normalized the REE pattern of the majority for examined specimens, regardless of comparatively high Th, Ti, Sc, Al, and REE content, showing seawater- like the REE structures in depletion of LREE, HREE enrichment, as well as minor positive La and Eu anomalies (Figs. 4 and 6a), each of which indicates elementary preserving of the seawater signals (Deng et al., 2017; Ozyurt et al., 2020). The remainder of the specimens, defined by the commonly documented MREE-bulge or hat-shaped patterns (Fig. 6b), are similarly unlikely for having been affected by siliciclastic elements since they had fewer total Al, Th, and REE concentrations than stratigraphically nearby specimens (Fig. 4). Geochemical thresholds are regarded as random and should thus be utilized on an individual basis for various testing (Tostevin, 2021). Some specimens had non-seawater like REE patterns and greater concentrations in terrigenous inputs proxies exceeding the threshold (Figs. 4 and 6b); additional strong data imply that contamination from the dissolving of terrigenous debris throughout the HAC leach procedure is negligible. As a result, fluids with high water-insoluble elements liberated from clays originating from continental weathering in early diagenesis might represent the major system, as predicted in several earlier studies (Zhao & Zheng, 2014; Hood et al., 2018).

Due to their structural integration with carbonate and the relatively low REE/Ca ratios in diagenetic liquids, the seawater REE pattern and associated Ce/Ce* in limestone are thought to have been less vulnerable to post-depositional change, thus being accurately maintained (Hood et al., 2018; Zhang & Shields, 2022). Nevertheless, consideration needs to be exercised when employing water-insoluble elements for tracking the paleo-seawater structure, particularly in situations in which carbonate is impure or siliciclastic contaminants are evident. For the current investigation, the vast majority of the specimens have seawater-like REE patterns that provide solid proof that the main Ce/Ce* was conserved. Though modest REEs have been released by siliciclastic constituents in early diagenesis, the Ce shows a poor association with Th (R^2 = 0.51; Fig. 7a), as well as a weak relationship with Mn (R^2 = 0.37; Fig. 7b). Furthermore, Mn shows weak and no connection with Th (R^2 = 0.27; Fig. 7c) and Sc (R^2 = 0.28; Fig. 7d), respectively. These data show the Ce fingerprint is significantly associated with redox-sensitive Mn actions, but neither is appreciably changed in interacting with siliciclastic detritus in earlier diagenesis.

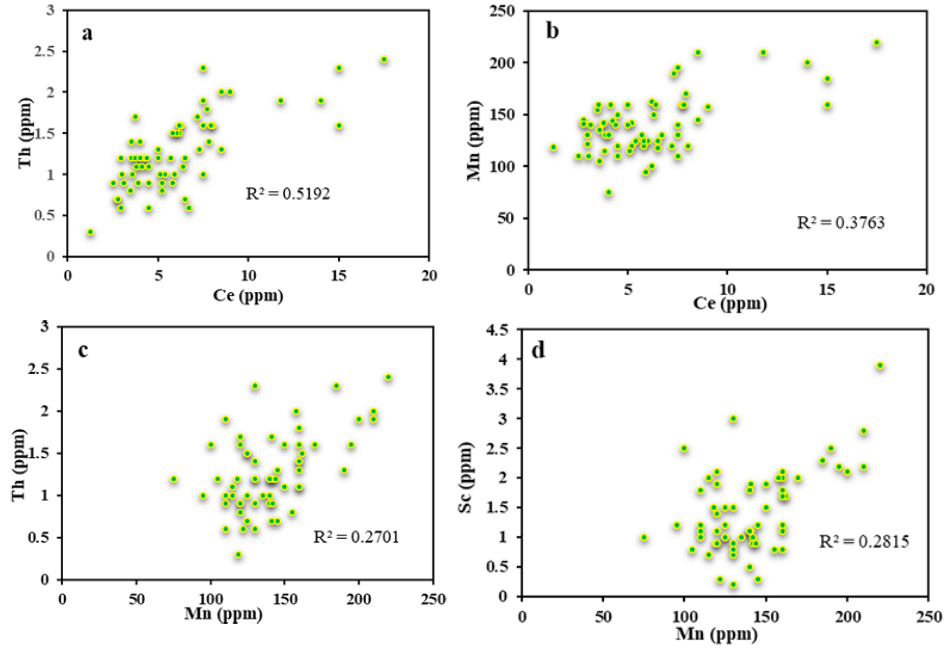

Figure 7. Cross-plots of components extracted from acetic acid (HAc, 1 N)-leaching liquid. Ce (a, R^2 = 0.5192); Mn (b, R^2 = 0.3763); Mn vs Th (c, R^2 = 0.2701) and Sc (d, R^2 = 0.2815).

5.2. Climate-mediated accelerated continental weathering throughout the Coniacian-Early Santonian

In the EB10 section, continental weathering as indicated by water-insoluble elements (Ti, Th, Sc, and REE) began rising around OAE3 border time, maintained very stable levels or only increased little during the OAE CIE's negative phase, as well as slowly came back to baseline levels over the recovery stage of the CIE (Fig. 4). Variations in paleoclimate and tectonism are the two main factors affecting continental weathering and hence related to terrigenous influx into marine by rivers (Mansour et al., 2022). In the Coniacian–Early Santonian period, the Baghdad Basin was a developed, tectonically quiet passive continental margin situated on a central coastal strip parallel to the Tethys Ocean's southwest side (Al-Hamdani, 1986; Mahdi et al., 2022). Therefore, it seems unlikely that the rise in continental weathering within the study region was primarily caused by uplift and regional tectonism. The most severe climatic and environmental disruptions were observed throughout the Upper Cretaceous, as evidenced by the OAE CIE and the earlier Coniacian–Early Santonian Boundary Event. These events were connected to the emplacement of deep ocean deposits, or Balambo strata (Al-Ameri & Al-Obaydi, 2011). Terrigenous influx may have grown due to greater physical weathering brought on by a sea level drop at a time of global cooling or increased chemical weathering at a time of global warming. Previous research indicates that a short-term transgressive pulse coincided with the OAE3, which was quickly followed by a potential modest decline in sea level, then, at the start of the OAE CIE, a rapid rise in sea level with a large amplitude (Immenhauser, 2005; Wendler, 2013; Kaya et al., 2020; Wagreich & Mansour, 2022). However, organic carbon analysis in the southern Tethys only revealed the sea-level rise linked to the OAE CIE (Mansour & Wagreich, 2022; Lawa et al., 2023). Based mostly on TEX_{86} compilations and global stable oxygen isotopes ($\delta^{18}O$), low-to-high latitude paleotemperature predictions of the Late Cretaceous show a comparable pattern, with extreme warmth throughout the Cenomanian-Turonian (Lawa et al., 2023), certain improvement but maintained warmth during the Coniacian-Santonian, while progressive warming expands within the Campanian along with the Maastrichtian (Huber et al., 2002; MacLeod et al., 2005; Friedrich et al., 2012; O'Brien et al., 2017; Mohammed et al., 2022). The EB10 section's steady rise in water-insoluble elements, however, does not line up with any suggested cycles of transgression and regression in sea level throughout the OAE3-OAE CIE timeframe. Thus, increasing terrigenous influx throughout the Coniacian-Santonian could not have been caused by shifts in sea level. Given that the rise in terrigenous influx wasn't primarily driven by a decline in sea level, the probable reason could be the chemical weathering linked to worldwide warming and the ensuing movement of these materials into seawater. According to oxygen-isotope rates in planktonic foraminifera, warming globally began at the OAE3 boundary in time and persisted until the OAE CIE (Huber et al., 2018).

In addition to the Os and Sr -isotope profile at sections of East Asia and Egypt (Figs. 5 and 8; Jenkyns, 2010; Cumming et al., 2012; Munier et al., 2023; Ali, 2023), this paleotemperature growth is tentatively compatible with the time of growing levels and peaking of water-insoluble components showing accelerated chemical weathering (Fig. 4). The Coniacian–Santonian period's synchronized alterations of these isotopes and element proxies of continental weathering imply that swift global warming caused an increase in this phenomenon worldwide, including the Southern Hemisphere's tropical region (Fig. 9A–C). Furthermore, these proxies' recovery to baseline levels throughout the CIE's phase of recovery was similarly synchronous, implying that increased organic carbon buried may have progressively reduced the CO_2 concentration and related intensity of continental weathering (Fig. 9D). It is possible to attribute the ongoing rise in Al throughout the recovery OAE3 period to factors other than the increasing influx of continental weathering, such as additional contributions from authigenic cycles. To increase the concentration of Al, for instance, biogenic silica could be transformed into authigenic aluminosilicates (DeMaster, 2003). This process allows the Al to be liberated and absorbed into carbonate. Two short-term increases in water-insoluble element trends were recorded layered above compared to the CIE interval (2055–2067 m and 2037–2045 m) (Fig. 4), which may indicate a further pulse of accelerated continental weathering. The EB10 section has not, however, shown equivalent sedimentary or carbon-isotope shifts over these two intervals, and the sections at southern Tethys (Egypt) and pelagic shelf sea (Eastbourne) do not appear to have seen noticeable shifts in multiple proxies after the OAE-CIE (Fig. 5). Consequently, based on the available data, it is probable that these two elemental rise pulses in the EB10 section are local signals whose origin is unclear.

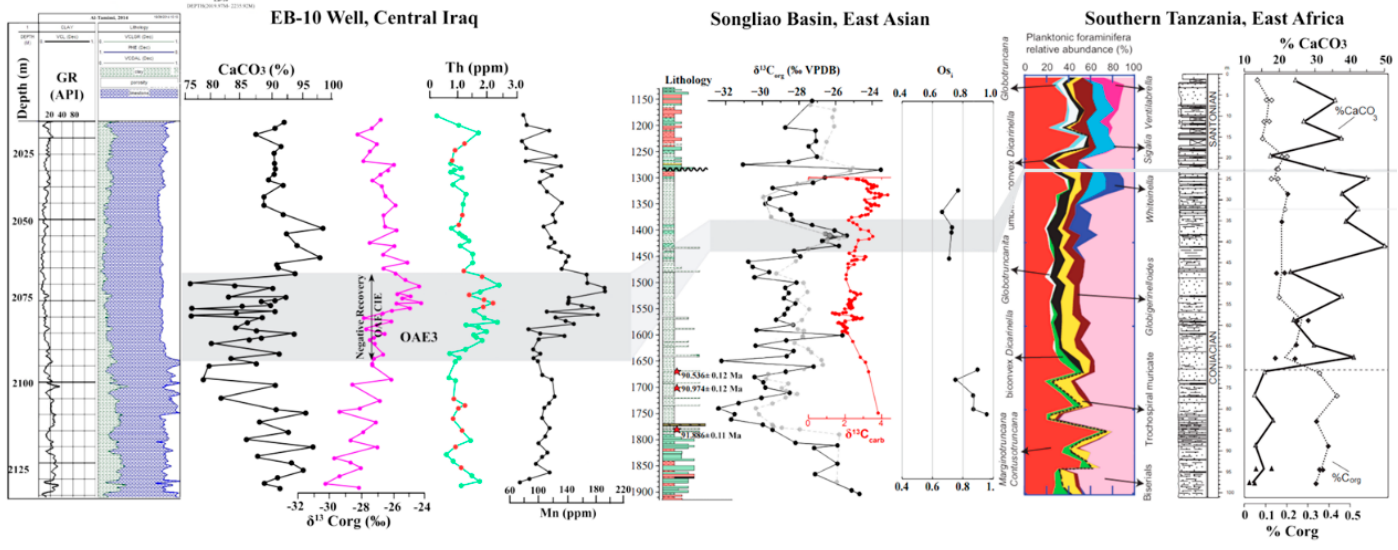

Figure 8. A systematic paleoenvironmental analysis from the Tanuma Carbonate Platform in Central Iraq, the Songliao Basin in East Asia, and Southern Tanzania in East Africa during the Coniacian-Santonian Age. Chemostratigraphic data from SK1-S core covering the upper Quantou through the Yaojia formations in the Songliao Basin. Column of stratigraphy adapted from Wu et al (2013). According to Wang et al. (2016), red stars are bentonite horizons with CA-ID-TIMS U/Pb zircon ages. Feng et al. (2010) identified a pause at the Qingshankou/Yaojia contact. Chamberlain et al. (2013) provided the red $\delta^{13}C_{carb}$ data, whereas Hu et al. (2015) provided the faded gray $\delta^{13}C_{org}$ values. Tanzania Drilling Project (TDP) Site 39's lithostratigraphy and chemostratigraphy from Petrizzo et al. (2017).

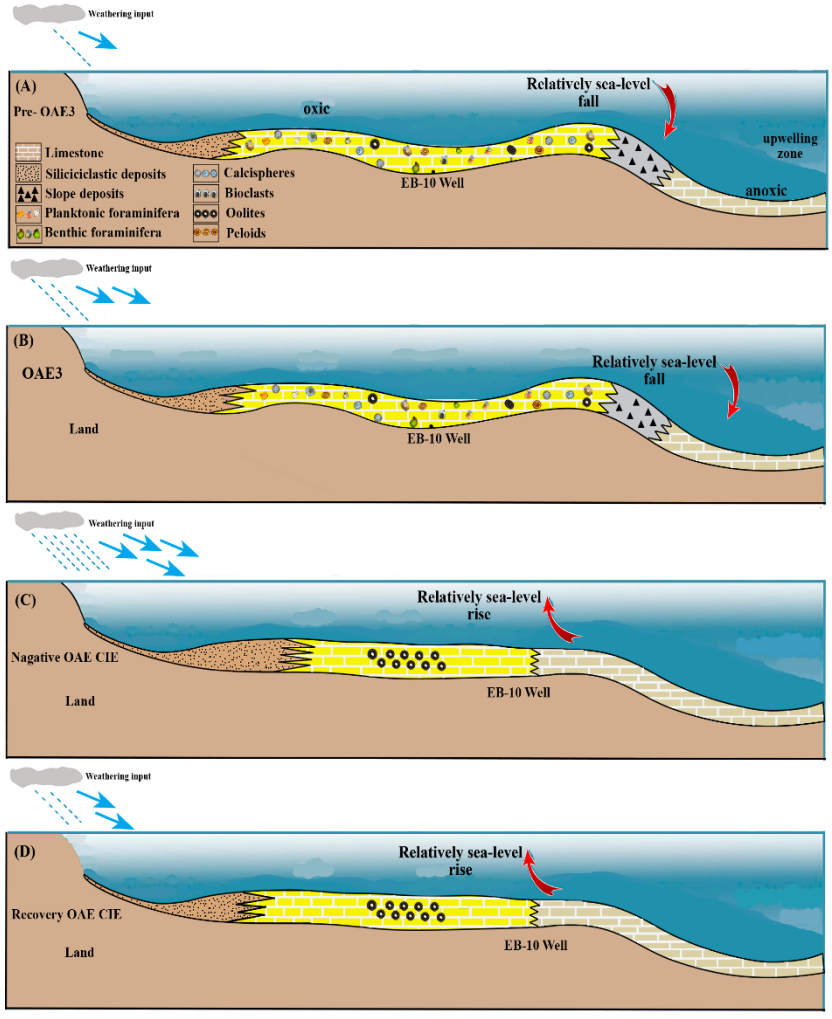

Figure 9. Reconstructions offering an understanding of the changes in continental weathering and deoxygenation during the OAE3 transition period at the shallow-water Tanuma Carbonate Platform in contemporary Central Iraq. Take note of the following: (1) The depositional environment abruptly changed in shallow-water carbonate platforms (A & B) to more deep water ramps (C & D) as a result of the increasing sea level rise with carbonate platforms crises during the initial phase during a OAE-CIE. (2) Growth of depleted in oxygen water is indicated by the arrows in red.

5.3. Shallow water redox conditions during the Coniacian–Santonian

In the shallow-water carbonate depositional setting, Mn and Ce are commonly employed for tracking intermediate manganous (suboxic) instead of completely anoxic conditions. This is due to their susceptibility to regional –local redox conditions (Jenkyns, 2010; Cao et al., 2020; Lan & Long, 2023). In the event that bottom waters become oxygenated, Mn is carried to the seafloor as Mn^{3+}/Mn^{4+} integrated into oxides (oxyhydroxides); conversely, in the event that oxygen levels depleted, the Mn oxides (oxyhydroxides) that were previously deposited have been reduced into soluble Mn^{2+} then integrated into early diagenetic carbonate crystal structures (Li et al., 2022). Ce^{3+} can oxidize to insoluble Ce^{4+}, which can then build up on the surface of organic and clay particulates, Mn oxides (oxyhydroxides), and isolated Ce oxide particulates in an oxygenated environment. This causes negative Ce/Ce* and Ce depletion in seawater (Loges et al., 2012). Contrarily, in a suboxic environment with low O_2, insoluble Ce^{4+} is converted to soluble Ce^{3+} and discharged to the water columns, resulting in a positive Ce/Ce* ratio and Ce enrichment. Thus, an increase in the concentration of Mn and Ce in the sediment and a positive Ce/Ce* ratio are widely regarded as essential stratigraphic markers for OAEs. These markers have been seen for the T-OAE, or oceanic anoxic events (Lu et al., 2010; Jenkyns, 2010; Tessin et al., 2015). A more sensible range of > 1.2 and < 0.8 is used in numerous investigations instead of the commonly accepted limit number of 1 to indicate positive and negative Ce/Ce*, which denote conditions below and above the Mn redoxcline, respectively, and oxygen-rich waters (Tostevin, 2021 and the references within it). Since the results in this study primarily fall in the range of 1.2 and 0.8, indicating little impact on Ce/Ce*, as shown in Figure 5, just the overall trend is reported below.

Mn (1.23º V) and Ce (1.61º V) have different reduction potentials, but both are susceptible to moderate manganous situations, and their redox cycle may act similarly in low oxygen environments. Figs. 5 and 7 show that there is, in fact, the anticipated positive association between these. The carbonate content of EB10 is adversely correlated with the levels of both of these components (Fig. 8 in the research), SK1-S core, and Abu Roash Member (Jones et al., 2018; Mansour et al., 2020b), respectively, despite the fact that carbonate forms the host phases and a rise in its amount may result in positive contributions for the values of Mn and Ce. As a result, the sediment's carbonate concentration does not dominate its enrichment of those minor elements. In an effort to reconstruct supra-regional or possibly global redox situations in shallow oceans, we contrast the collected Mn and Ce information from the present investigation (Fig. 5) with equivalent proxies at other sites in Eastbourne (pelagic shelf sea) and Qingshankou Members 1 and 2 -3 in the SK1-S core in East Asian waters (Lu et al., 2010; Jones et al., 2018). This depends upon the distinctive negative CIE throughout the OAE3 transitional period plus OAE CIE. High-resolution

measurements of Ce/Ce*, Ce, and Mn generally at the EB10 well indicate a consistent increase that begins near the OAE3 boundary and ends in the OAE CIE at the end level. Within a similar stratigraphic range, there is a generalized positive shifting of Ce/Ca and Mn/Ca, with Ce anomalies of southern England (Eastbourne) (Lu et al., 2010) also for Mn of the SK1-S core in East Asia (Jones et al., 2018). These profiles do not, however, exhibit the declining trend that would be expected given the CIE's middle values; this discrepancy may be due to local or poor resolution issues. An improved global fixing of Ce and Mn, likely the result of a single primary pulse that lasted the entire Coniacian–Early Santonian, is shown by the matching variations in Ce/Ce*, Ce, Mn, Sr, and I/Ca, Ce/Ca, Ce anomaly, and Mn/Ca from the globally separating locations of shallow water carbonate platforms for EB-10 (Central Iraq), Abu Roash Formation (Egypt) (southern Tethys), and the pelagic shelf sea of Eastbourne (intersection of the proto-Atlantic and westernmost Tethys). These data imply that, beginning near the boundary of OAE3 and going on, although with occasional variations, during the CIE period, depleted-oxygen (manganous) bottom waters at least spread throughout some Tethyan continental boundaries during the Coniacian-Early Santonian (Figs. 8 and 9A-D). According to recent research by März et al. (2009) using redox-sensitive components in bulk rock on the Late Cretaceous carbonates of the Demerara Rise, oxygen-depleted seas in this region spread into shallow water levels (Fig. 1). Within this setting, a major source of the diagenetic integration of these ions inside the carbonate lattice may have been the dissolution of Ce^{3+} and Mn^{2+} at Mn oxides (oxyhydroxides) and the reduction of Ce oxides from earlier deposits. The image that results is thus one of Ce and Mn enrichment caused by global redox shift impacting comparatively shallow tropical water in the Coniacian-Early Santonian platform carbonates in the wider Tethyan basin. A deoxygenated global ocean is suggested from the OAE3 boundary period upward, as indicated by coeval positive in S of carbonate-associated sulphates from sections at ODP Site 1261 (Demerara Rise) (Fig. 10), pelagic shelf sea, Eastbourne (März et al., 2009; Jenkyns, 2010; Mansour & Wagreich, 2023). Significantly, Ce isotopes exhibit one positive shift at the identical stratigraphic period as the Mn and Ce/Ce* excursions in the EB-10 section, as determined by the T-OAE CIE correlation. This is thought to be the result of a significant decrease in worldwide Mn oxide (oxyhydr) depositing, which also liberated the heavier Ce isotope that had been adsorbed. Isotopic systems' interpretations regarding the significance of a global redox postdating to the CIE are unclear because the S and Th isotopes do not later recover to background values. On the other hand, Tessin et al. (2015) found that the Mn enrichment on the Portland core (English Channel) happened around the OAE3 boundary period and reverted to background values after the CIE started. This trend is stratigraphically related to the first enhancing Mn phase observed at EB10 and the Late Cretaceous carbonate of the Eastbourne. The data from the EB-10 well and pelagic shelf water in Eastbourne, where the Mn content recovers to baseline near the end level in the CIE (Fig. 5), does not correspond with this early recovery and may instead point to a local signal. The OAE3 boundary is the stratigraphically closest point below which the redox-sensitive elements begin to grow, as per the latest data gathered for this investigation (Figs. 4, 5, and 8). This discrepancy in chronology suggests that increased continental weathering & inputs of nutrients may have contributed to the first event of shallow-water deoxygenation. This enhanced primary productivity resulted in a large consumption of oxygen, which was most noticeable in the deeper regions of the platform. The data indicate high hydrocarbon potential in specific intervals.

On the other hand, during the CIE's recovery phase, the progressive decrease in water-insoluble components is accompanied by an increase in redox-sensitive elements. An upward trend of Tl isotopes and a shift to lower radiogenic levels of Os isotopes over this geologic era are the patterns that align with a coeval connection in isotopic data (Cohen et al., 2004; Jones et al., 2018). Therefore, this deoxygenation episode cannot be explained by the accelerated continental weathering process (Fig. 9D). Notably, this time frame aligns with the high-temperature conditions encapsulated in a worldwide compilation of benthic foraminiferal oxygen-isotope ($\delta^{18}O$) data, and the TEX_{86} temperature proxy has been extensively utilized in Cretaceous environments (O'Brien et al., 2017). In addition to significantly contributing to the drop in solubility of oxygen, such extreme temperatures may have promoted water column stratification and slowed circulation. On the other hand, better recirculation of bioessential nutrients in increasingly decreasing environments may have induced a rise in primary productivity and oxygen depletion.

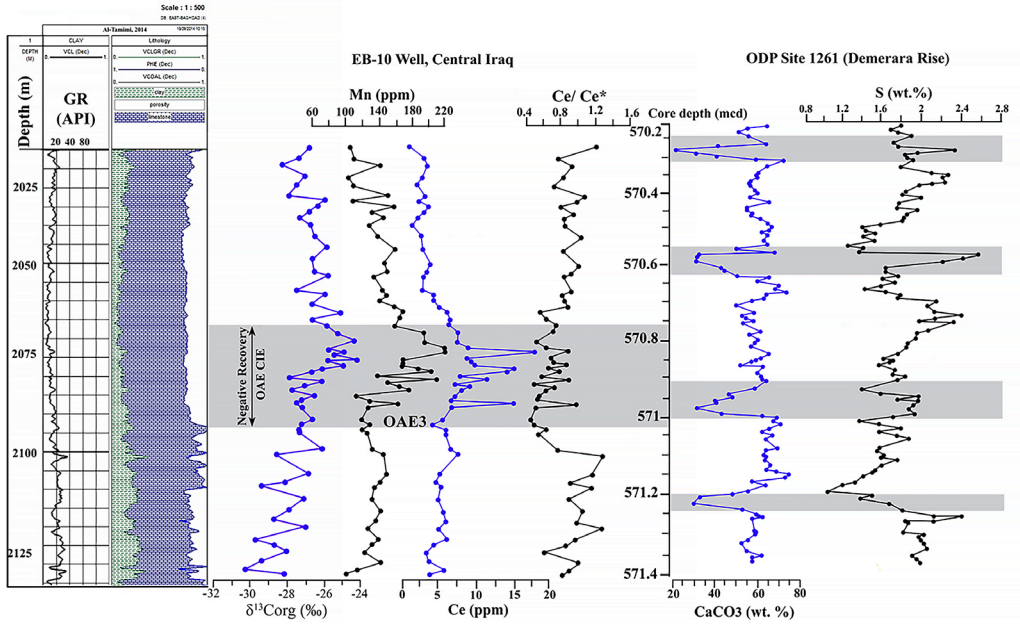

Figure 10. The correlation for geochemical profiles for widely employed redox proxies at Coniacian-Early Santonian carbonates from the EB-10 Well (Central Iraq) and Demerara Rise (NW South American margin). $CaCO_3$ and S data for the Late Cretaceous carbonates of the Demerara Rise at Site 1261 are from März et al. (2009).

5.4. Enhanced oxygen depletion and continental weathering are linked with the carbonate crisis.

In the Tanuma Carbonate Platform's subtropical Tethys Ocean during the OAE3 Late Cretaceous, bioclasts, oolites, and peloids, as well as other benthonic and planktonic faunas (Rotalid, Textularid, Miliolid, Globigerinid foraminifera, etc.), multiplied and created significant depositional systems (Aqrawi, 1996; Al-Ameri & Al-Obaydi, 2011; Ali et al., 2022; Fig. 9A, B). Major carbonate-platform crisis episodes occurred at the Coniacian–Early Santonian and OAE3 boundary times along the northern Tethyan edge (Wendler et al., 2009; Phelps et al., 2015; Mansour & Wagreich, 2022). Biological extinction and a clear decrease in carbonate composition serve as clear examples of the carbonate production crisis. The $CaCO_3$ (2095–2093 m) in the EB10 well shows a consistent downward trend from ~87.5–83.5%, which corresponds with the OAE CIE start interval. This is followed by many times of sharp fall from ~94–76%, which corresponds to the CIE negative phases itself (2067–2093 m; Fig. 8). According to the most current data from the Tanuma Platform, the skeleton grain content and foraminiferal variety began to decline at the OAE3 border and declined more sharply throughout the OAE CIE's negative phase (Figs. 3 and 8). There is no other notable calcareous microfossil or nannofossil datum close to this level (CIE); the lowest rare Dicarinella asymetrica planktonic foraminifers and Lucianorhabdus cayeuxii nannoplankton are found much below (Aqrawi, 1996; Remin, 2004; Haddad & Amin, 2007; Gale et al., 2007; Fig. 9C). Despite the serious benthic fauna crisis that the Tanuma Platform experienced, some smaller foraminifers continued to be visible as sediment growers throughout the CIE interval, and the resulting facies still have an elevated $CaCO_3$ content, indicating that the biotic platform was not entirely closed down despite pressure (Fig. 9C, D). In general, it is likely that the environmental disruptions at the OAE3 boundary period only slightly altered the Tanuma carbonate factory, but they were a crucial contributor in the ensuing late Cretaceous benthic biological crisis of carbonate growers. The findings in global locations ranging from hemipelagic and shallow marine environments are consistent with this growing crisis in carbonate production (Mansour & Wagreich, 2022). On the contrary, in the Sinai Desert (Egypt) and Kopet-Dagh Basin (NE Iran), there is data of a considerable fall in $CaCO_3$ amount and an abrupt transition of carbonate to siliciclastic deposition at the Coniacian-Santonian boundary, indicating that most carbonate factories essentially shut down at this boundary (Kalanat et al., 2021; Bomou et al., 2023). In fact, some bio carbonate platforms did indeed disappear around the Coniacian-Santonian boundary, but other robust platforms persisted and gave rise to relatively non-fossiliferous oolitic sedimentary formations or weakly fossiliferous submerged micrites (Yilmaz et al., 2018; Steuber et al., 2023). There are a number of non-exclusive explanations for the global crisis in carbonate production, such as greater terrigenous input, eutrophication, temperature excess, rise in sea levels, oceanic oxygen depletion and acidification (Jenkyns, 2010; Han et al., 2022). But throughout the Coniacian–Early Santonian, these processes likely had varying roles in various basins throughout time periods and typically worked in combination with local influences. The OAE CIE (Fig. 8) shows a strong correlation between the rapid rise in sea level and platforms crisis in EB10, which includes living things and carbonate production. However, the rate of carbonate deposition on a robust and abundant platform ought to have been sufficient to keep up with the increase in the level of the sea (Yilmaz et al., 2018). According to the results of this investigation, an increase in Ti, Al, Th, Sc, and REE at Tanuma Platform precedes a rise in Mn, Ce, and Ce/Ce*; this increase initially appears at the OAE3 border (Figs. 4, 5, and 8). Thus, it is likely that the marginal decline in foraminiferal variety, carbonate content, and skeleton abundance in Central Iraq was caused by the almost simultaneous augmented terrigenous input and deoxygenation during this time period (Fig. 8). The macrobenthic populations, which include benthic foraminifera (Figs. 3 and 8) and carbonate content (Figs. 4, 8, and 9A-C), present a substantial drop, indicating a corresponding carbonate-platform crisis, after these proxies exhibit a synchronized fast wide rise at the initial degree of the OAE CIE. The correlation between these findings and the significantly increased terrigenous input and deoxygenation in response to the late Cretaceous significant release of carbon rhythm suggests that these processes were probably crucial in degrading ecosystems and initiating a biological crisis for the benthic carbonate growers. Because observable siliciclastic deposits were found in Sinai around the OAE3 boundary and in the Coniacian–Early Santonian period (Bauer et al., 2003; Mansour & Wagreich, 2022), yet not in Central Iraq, it is evident that the terrigenous influx in carbonate platforms exhibited significant local heterogeneity. Finding specific geochemical proxies of terrigenous input (REE, Sc, Th, Ti, and Al) of isolated carbonate platforms—such as China, Hungary, and Egypt in the northern and southern Tethys—that weren't directly affected by continental rivers inputs is necessary, as this study demonstrates, in order to evaluate potential global resemblance. Redox proxies on the Tanuma Platform and the Adriatic Carbonate Platform region (such as Eastbourne; Lu et al. 2010) have altered, suggesting that oxygen depletion within shallow water prior to or concurrent to the biologic carbonate platforms crisis was probably widespread along the southern Tethyan margin. This could have had extremely detrimental effects on carbonate generators and sediment formation.

6. Conclusions

Determining possible triggers of the carbonate production crisis and offering special insight into palaeoceanographic modifications to shallow tropical waters throughout the Coniacian-Santonian period are two benefits of analyzing the trace and major elements found in carbonates at the Tanuma carbonates platform in Central Iraq. The majority of elements insoluble in water (like REE, Sc, Th, Ti, and Al) have risen synchronously, beginning at the OAE3 boundary and going on through the OAE CIE's negative phase. This indicates the warming temperatures, along with raised continental weathering, have probably caused improved terrigenous influx to the shallow marine system. Immediately after the rise in water-insoluble elements starts, there is a modest enrichment in Ce, Mn, and Ce/Ce*. Then, as water-insoluble elements increase during the negative stage in the OAE CIE, this enrichment moves stratigraphically upward in higher levels through time. These data support the idea that, in this time period, deoxygenation of shallow waters may have been associated with increased continental weathering with nutrient inputs, supporting comparatively high primary production and consumption of oxygen. In the recovery phase of CIE, on the other hand, the water insoluble components exhibit a gradually declining trend superimposed on a positive shifting for redox proxies. There are several possible explanations for this deoxygenation, including localized stratification of the water columns and improved recycling of bioessential nutrients with elevated primary productivity. The Tanuma carbonate factory was likely slightly modified around the OAE3 boundary time due to the association between carbonate levels and proxies over terrigenous flow and the deoxygenation and biologic data of skeletal grain content. This modification probably played a crucial part in the Coniacian–Early Santonian crisis that benthic carbonate producers faced, which worsened as the OAE negative the CIE coincided. Another coeval carbonate platform located in western Tethys could possibly benefit from a similar process.

Acknowledgements

The core samples, information, and reports were supplied by the Midland Oil Company of Iraq (Md.O.C.), for which the author is appreciative. Much gratitude and appreciation are owed to the University of Baghdad's Department of Geology's authority and mineralogical laboratory staff for their help in getting the thin sections ready.

Formatting of funding sources

This research did not receive any specific grant from funding agencies in the public, commercial, or not-for-profit sectors.

Declaration of competing interest

The authors declare that they have no known competing financial interests or personal relationships that could have appeared to influence the work reported in this paper.

References

Abdel-Fattah, M. I., Mahdi, A. Q., Theyab, M. A., Pigott, J. D., Abd-Allah, Z. M., & Radwan, A. E. (2022). Lithofacies classification and sequence stratigraphic description as a guide for the prediction and distribution of carbonate reservoir quality: a case study of the Upper Cretaceous Khasib Formation (East Baghdad oilfield, central Iraq). Journal of Petroleum Science and Engineering, 209, 109835. https://doi.org/10.1016/j.petrol.2021.109835

Al-Ameri, T. K. & Al-Obaydi, R. Y. (2011). Cretaceous petroleum system of the Khasib and Tannuma oil reservoir, East Baghdad oil field, Iraq. Arabian Journal Geosciences, 4, 915–932. https://doi.org/10.1007/s12517-009-0115-4

Al-Ameri, T. (2011). Khasib and Tannuma oil sources, East Baghdad oil field, Iraq. Marine and Petroleum Geology, 28(4): 880-894. DOI:10.1016/j.marpetgeo.2010.06.003

Al- Hamdani, A.M. (1986). Stratigraphy and geochemistry of Khasib, Tanuma and Saadi Formations in East Baghdad Oilfield, Central Iraq. Ph.D. Thesis (unpublished), College of Science, University of Baghdad.

Algouti, A., Algouti, A., Hadach, F., Farah, A. & Aydda, A. (2023). Upper Cretaceous deposits on the Northern side of the High Atlas Range of Marrakesh (Morocco): tectonics, sequence stratigraphy and paleogeographic evolution. Boletin de la Sociedad Geologica Mexicana, 74 (1). https://doi.org/10.18268/bsgm2022v74n1a101121

Ali, R.A. & Jassim, H.K. (2023). Sedimentology and geochemistry of Zubair Formation sandstone reservoir, East Baghdad Oilfield, central Iraq. Kuwait Journal of Science, *50(3),* 427-437. https://doi.org/10.1016/j.kjs.2023.01.006

Ali, R.A., (2023a). Geochemistry and paleoredox conditions of the carbonate reservoir Khasib Formation in East Baghdad Oilfield-Central Iraq. Journal of Petroleum Research and Studies, 41, 16-36. DOI: https://doi.org/10.52716/jprs.v13i4.757

Ali, R.A. (2023b). Dolomitization mechanism of Pila Spi formation (middle-late eocene) in the high folded zone, Northern Iraq. Kuwait Journal of Science, *50(2),* 105-114. https://doi.org/10.1016/j.kjs.2023.02.015

Ali, H., Maziqa, F.H. & Al-Owaidi, M. (2022). A stratigraphic analysis of the Khasib, Tanuma and Sa'di Formations in the Majnoon Oil Field, Southern Iraq. *Bulletin* of the *Geological Society* of *Malaysia*, 73(1):163-169. http://dx.doi.org/10.7186/bgsm73202213

Aqrawi, A.A. (1996). Carbonate-siliciclastic sediments of the Upper Cretaceous (Khasib, Tanuma and Sa'di Formations) of the Mesopotamian Basin. Marine and Petroleum Geology, 13(7), 781-790. https://doi.org/10.1016/0264-8172(96)00022-0

Andrieu, S., Krencker, F.-N. & Bodin, S. (2022). Anatomy of a platform margin during a carbonate factory collapse: implications for the sedimentary record and sequence stratigraphic interpretation of poisoning events. Journal of the Geological Society, 179. https://doi.org/10.1144/jgs2022-005

Bauer, J., Kuss, H-J. & Steuber, T. (2003). Sequence architecture and carbonate platform configuration (Late Cenomanian–Santonian), Sinai, Egypt. Sedimentology, 50(3): 387 – 414. DOI:10.1046/j.1365-3091.2003.00549.x

Blättler, C., Jenkyns, H.C., Reynard, L. & Henderson, G.M. (2011). Significant increases in global weathering during Oceanic Anoxic Events 1a and 2 indicated by calcium isotopes. Earth and Planetary Science Letters, 309(1):77-88. DOI:10.1016/j.epsl.2011.06.029

Bomou, B., Adatte, T., Kaenel, E.D., Spangenberg, J., Gertsch, B., and Föllmi, K.B. (2013). Is the Coniacian-Santonian OAE3 a real and global anoxic event? Insights from Spain, Texas and Egypt, EGU2013-9898, 2013: EGU General Assembly, Vienna, 15.

Bomou, B., Adatte, T. & Spangenberg, J.E. (2023). Palaeoenvironmental and palaeontological study of the Gabal Ekma Section (Egypt) throughout the Coniacian-Santonian boundary. Advances in Science, Technology& Innovation, 291- 304. https://www.springer.com/series/15883

Brazier, J.M., Suan, G., Tacail, T., Simon, L., Martin, J.E., Mattioli, E. & Baiter, V. (2015). Calcium isotope evidence for dramatic increase of continental weathering during the Toarcian oceanic anoxic event (Early Jurassic). Earth and Planetary Science Letters, 411, 164–176. DOI:10.1016/j.epsl.2014.11.028

Cao, H., Kaufman, A.J., Shan, X., Cui, H. & Zhang, G. (2016). Sulfur isotope constraints on marine transgression in the lacustrine Upper Cretaceous Songliao Basin, northeastern China. Palaeogeography, Palaeoclimatology, Palaeoecology, 451, 152-163. https://doi.org/10.1016/j.palaeo.2016.02.041

Cao, C., Liu, X.-M., Bataille, C.P. & Liu, C. (2020). What do Ce anomalies in marine carbonates really mean? A perspective from leaching experiments. Chemical Geology, 532, 119413. https://doi.org/10.1016/j.chemgeo.2019.119413

Cao, H., He, W., Chen, F., Shan, X., Kong, D. & Hou, Q. (2021). Integrated chemostratigraphy ($\delta^{13}C$-$\delta^{34}S$-$\delta^{15}N$) constrains Cretaceous lacustrine anoxic events triggered by marine sulfate input. Chemical Geology, 559, 119912. https://doi.org/10.1016/j.chemgeo.2020.119912

Chamberlain, C. P., Wan, X., Graham, S.A., Carroll, A.R., Doebbert, A.C., Sageman, B.B., Blisniuk, P.,Kent-Corson, M.L., Wang, Z. & Chengshan, W. (2013). Stable isotopic evidence for climate and basin evolution of the Late Cretaceous Songliao basin, China. Palaeogeography, Palaeoclimatology, Palaeoecology, 385, 106–124. https://doi.org/10.1016/j.palaeo.2012.03.020

Chen, Xi, Wang, C., Wu, H., Kuhnt, W., Jia, J., Holbourn, A., Zhang, L. & Ma, C. (2015). Orbitally forced sea-level changes in the upper Turonian–lower Coniacian of the Tethyan Himalaya, southern Tibet. Cretaceous Research, 56, 691-701. https://doi.org/10.1016/j.cretres.2014.07.010

Chenot, E., Deconinck, J-F, Pucéat, E. & Pellenard, P. (2018). Continental weathering as a driver of Late Cretaceous cooling: new insights from clay mineralogy of Campanian sediments from the southern Tethyan margin to the Boreal realm. Global and Planetary Change, 162, 292-312. https://doi.org/10.1016/j.gloplacha.2018.01.016

Clarkson, M. O., Stirling, C. H., Jenkyns, H. C., Dickson, A. J., Porcelli, D., Moy, C. M., Pogge von Strandmann, P.A.E., Cooke, I.R. & Lenton, T.M. (2018). Uranium isotope evidence for two episodes of deoxygenation during Oceanic Anoxic Event 2. Proceedings of the National Academy of Sciences, 115(12), 2918–2923. https:// doi.org/10.1073/pnas.1715278115

Cohen, A.S., Coe, A.L., Harding, S.M. & Schwark, L. (2004). Osmium isotope evidence for the regulation of atmospheric CO_2 by continental weathering. Geology, 32, 157–160.DOI: https://doi.org/10.1130/G20158.1

Cumming, V.M., Selby, D. & Lillis, P.G. (2012). Re–Os geochronology of the lacustrine Green River Formation: Insights into direct depositional dating of lacustrine successions, Re–Os systematics and paleocontinental weathering. Earth and Planetary Science Letters, 359–360: 194-205. https://doi.org/10.1016/j.epsl.2012.10.012

Dameron, S.N., Leckie, R.M., Clark, K., MacLeod, K.G., Thomas, D.J. & Lees, J.A. (2017). Extinction, dissolution, and possible ocean acidification prior to the Cretaceous/Paleogene (K/Pg) boundary in the tropical Pacific. Palaeogeography, Palaeoclimatology, Palaeoecology, 485, 433-454. https://doi.org/10.1016/j.palaeo.2017.06.032

Deng, Y., Ren, J., Guo, Q., Cao, J., Wang, H. & Liu, C. (2017). Rare earth element geochemistry characteristics of seawater and porewater from deep sea in western Pacifc. Scientific Reports, 7: 16539. DOI:10.1038/s41598-017-16379-1

DeMaster, D. (2003). The diagenesis of biogenic silica: Chemical transformations occurring in the water column, seabed, and crust. Treatise on Geochemistry, 7, 87-98. https://doi.org/10.1016/B0-08-043751-6/07095-X

Fayadh, A.H. & Nasser, M.E., (2018). 3D geological model for Khasib, Tanuma, and Sa'di formations of Halfaya Oil Field in Missan Governorate-Southern Iraq. Iraqi Journal of Science, 59(2B), 875-885 DOI:10.24996/ijs.2018.59.2B.8

Feng, Z.-q., Jia, C.-z., Xie, X.-n., Zhang, S., Feng, Z.-h. & Cross, T.A. (2010). Tectonostratigraphic units and stratigraphic sequences of the non-marine Songliao basin, northeast China. Basin Research, 22, 79-95. DOI:10.1111/j.1365-2117.2009.00445.x

Franchi, F. (2018). Petrographic and geochemical characterization of the Lower Transvaal Supergroup stromatolitic dolostones (Kanye Basin, Botswana). Precambrian Research, 310. DOI:10.1016/j.precamres.2018.02.018

Friedrich, O., Norris, R. D., & Erbacher, J. (2012). Evolution of middle to late Cretaceous oceans – A 55 my record of Earth's temperature and carbon cycle. Geology, 40(2), 107–110. https://doi.org/10.1130/g32701.1

Gale, A.S., Kennedy, W.J., Lees, J.A., Petrizzo, M.R. & Walaszczyk, I. (2007). An integrated study (inoceramid bivalves, ammonites, calcareous nannofossils, planktonic foraminifera, stable carbon isotopes) of the Ten Mile Creek section, Lancaster, Dallas County, north Texas, a candidate global boundary Stratotype Section and point for the base of the Santonian Stage. Acta Geologica Polonica, 57 (2), 113-160.

Gharib, A. F., Ismael, J. I., Alatroshe, R. K., Farhan, H. N., Abdel-Fattah, M. I., & Pigott, J. D. (2024). Organic matter characteristics and hydrocarbon generation potential of the Middle Jurassic–Lower Cretaceous succession in the Mesopotamian Foredeep Basin, Iraq. International Journal of Earth Sciences, 113(8), 2163-2187. http://dx.doi.org/10.1007/s00531-024-02434-6

Haddad, S.N. & Amin, M.A. (2007). Mid-Turonian–early Campanian sequence stratigraphy of northeast Iraq. GeoArabia, 12 (2), 135–176. https://doi.org/10.2113/geoarabia1202135

Haq, B.U. (2014). Cretaceous eustasy revisited. Global and Planetary Change, 113, 44–58. https://doi.org/10.1016/j.gloplacha.2013.12.007

Han, Z., Hu, X., Hu, Z., Jenkyns, H.C. & Su, T. (2022). Geochemical evidence from the Kioto Carbonate Platform (Tibet) reveals enhanced terrigenous input and deoxygenation during the early Toarcian. Global and Planetary Change, 215,103887. https://doi.org/10.1016/j.gloplacha.2022.103887

Hood, A.V.S., Planavsky, N.J., Wallace, M.W. & Wang, X. (2018). The effects of diagenesis on geochemical paleoredox proxies in sedimentary carbonates. *Geochimica* et Cosmochimica *Acta,* 232, 265–287. DOI:10.1016/j.gca.2018.04.022

Hu, X., Wagreich, M. & Yilmaz, I. O. (2012). Marine rapid environmental/climatic change in the Cretaceous greenhouse world. Cretaceous Research, 38, 1–6. DOI:10.1016/j.cretres.2012.04.012

Hu, J.F., Peng, P.A., Liu, M.Y., Xi, D.P., Song, J.Z., Wan, X.Q. & Wang, C.S. (2015). Seawater incursion events in a Cretaceous paleo-lake revealed by specific marine biological markers. Scientific Reports, 5, 9508. DOI:10.1038/srep09508

Huber, B. T., Norris, R. D., & MacLeod, K. G. (2002). Deep-sea paleotemperature record of extreme warmth during the Cretaceous. Geology, 30, 123–126. https://doi.org/10.1130/0091-7613(2002)0302.0.co;2

Huber, B. T., MacLeod, K.G., Watkins, D.K. & Coffin, M.F. (2018). The rise and fall of the Cretaceous hot greenhouse climate. Global and Planetary Change, 1-23. https://doi.org/10.1016/j.gloplacha.2018.04.004

Immenhauser, A. (2005). High-rate sea-level change during the Mesozoic: New approaches to an old problem. Sedimentary Geology, 175, 277 – 296. doi:10.1016/j.sedgeo.2004.12.016

Jarvis, I., El Asmi, A.M., Moody, R.T.J. & Cabrera, S. (2002). Late Cretaceous (Campanian) carbon isotope events, sea-level change and correlation of the Tethyan and Boreal realms. Palaeogeography, Palaeoclimatology, Palaeoecology, 188(3-4): 215-248. https://doi.org/10.1016/S0031-0182(02)00578-3

Jenkyns, H.C. (2003). Evidence for rapid climate change in the Mesozoic–Palaeogene greenhouse world. The Royal Society, London, 361, 1885–1916. DOI: 10.1098/rsta.2003.1240

Jenkyns, H. C. (1980). Cretaceous anoxic events: from continents to oceans. Journal of Geological Society, 137(2):171-188. DOI:10.1144/gsjgs.137.2.0171

Jenkyns, H.C. (2010). Geochemistry of oceanic anoxic events. *Geochemistry*, *Geophysics*, *Geosystems,* 11, Q03004. https://doi.org/10.1029/2009GC002788.

Jones, C. E. (2001). Seawater strontium isotopes, oceanic anoxic events, and seafloor hydrothermal activity in the Jurassic and Cretaceous. *American* Journal of *Science,* 301, 112–149. DOI:10.2475/ajs.301.2.112

Jones, M. M., Ibarra, D. E., Gao, Y., Sageman, B. B., Selby, D., Chamberlain, C. P. & Graham, S. A. (2018). Evaluating Late Cretaceous OAEs and the influence of marine incursions on organic carbon burial in an expansive East Asian paleo-lake. Earth and Planetary Science Letters, 484, 41-52. DOI:10.1016/j.epsl.2017.11.046

Kalanat, B., Davtalab, E. & Vahidinia, M. (2021). The oxic Coniacian-Santonian interval in the Kopet-Dagh Basin (NE Iran): Carbon isotope and benthic-planktic foraminiferal assemblages at the time of the last Cretaceous OAE. Palaeogeography Palaeoclimatology Palaeoecology, 588(8):110817. DOI:10.1016/j.palaeo.2021.110817

Kaya, M.Y., Dupont- Nivet, G., Proust, J-N, Roperch, P., Meijer, N., Frieling, J., Fioroni, C., Altiner, S.O., Stoica, M., Aminov, J., Mamtimin, M. & Guo, Z. (2020). Cretaceous evolution of the Central Asian Proto- Paratethys Sea: Tectonic, eustatic, and climatic controls. AGU Advancing *Earth and Space Science,* 39(9), 1- 27. https://doi.org/10.1029/2019TC005983

Keller, G. (2008). Cretaceous climate, volcanism, impacts, and biotic effects. Cretaceous Research, 29(5-6), 754-771. https://doi.org/10.1016/j.cretres.2008.05.030

Korbar, T., Glumac, B., Tešović, B. C., & Cadieux, S. B. (2012). Response of a carbonate platform to the Cenomanian-Turonian drowning and OAE 2: A case study from the Adriatic platform (Dalmatia, Croatia) carbonate platform response to the Cenomanian-Turonian drowning and OAE 2. Journal of Sedimentary Research, 82(3), 163–176. https://doi.org/10.2110/jsr.2012/17

Labandeira, C., Rodríguez-Tovar, F.J. & Uchman, A. (2016). The End-Cretaceous Extinction and Ecosystem Change. Springer Link, in Book (The Trace-Fossil Record of Major Evolutionary Events), V. 2: Mesozoic and Cenozoic, 265–300. DOI:10.1007/978-94-017-9597-5_5

Lan, C. & Long, X. (2023). Redox-stratified seawater during the GOE: Evidences from rare earth elemental and C-O isotopic compositions of Paleoproterozoic BIF and carbonate rocks from the Taihua Group, North China Craton. Ore Geology Reviews, 157, 105424. https://doi.org/10.1016/j.oregeorev.2023.105424

Lash, G.G., 2018. Significance of stable carbon isotope trends in carbonate concretions formed in association with anaerobic oxidation of methane (AOM), Middle and Upper Devonian shale succession, western New York State, USA. Marine and Petroleum Geology, 91, 470e479. https://doi.org/10.1016/j.marpetgeo.2018.01.032

Lawa, F.A.A., Mohammed, I.Q., Farouk, S., Ahmad, F., Faris, M., Tanner, L.H. & El-Khahtany, K., (2023). Stratigraphic architecture of the Tethyan Cenomanian-Turonian succession and OAE2 in the Dokan Area, Kurdistan Region, northeast Iraq. Journal of African Earth Sciences, 207(2):105064. DOI:10.1016/j.jafrearsci.2023.105064

Lawrence, M. & Kamber, B. (2006). The behaviour of the rare earth elements during estuarine mixing--revisited. Marine Chemistry, 100. DOI: 147-161. 10.1016/j.marchem.2005.11.007.

Leckie, R. M., Bralower, T. J. & Cashman, R. (2002). Oceanic anoxic events and plankton evolution: Biotic response to tectonic forcing during the mid-Cretaceous. Paleoceanography, 17, 131–1329. DOI:10.1029/2001PA000623

Li, X.Y., Wang, E-J., Wu, C-Q., Zhao, D-H., Hua, B., Zhang, Z-W., Xu, J-H. & Jin, Z-R. (2022). The redox-conditions controlled manganese carbonate mineralization in the Late Paleozoic Qiaerlong deep basin, Western Kunlun Mountains, China. Ore Geology Reviews, 147, 104993. https://doi.org/10.1016/j.oregeorev.2022.104993

Loges, A., Wagner, T., Barth, M.G. & Bau, M. (2012). Negative Ce anomalies in Mn oxides: The role of Ce^{4+} mobility during water–mineral interaction. Geochimica et Cosmochimica Acta, 86:296–317. DOI:10.1016/j.gca.2012.03.017

Lowery, C.M., Leckie, R.M. & Sageman, B.B. (2017). Micropaleontological evidence for redox changes in the OAE3 interval of the US Western Interior: Global vs. local processes. Cretaceous Research, 69, 34-48. https://doi.org/10.1016/j.cretres.2016.08.011

Lu, Z.L., Jenkyns, H.C. & Rickaby, R.E.M. (2010). Iodine to calcium ratios in marine carbonate as a paleo-redox proxy during oceanic anoxic events. Geological Society of America, 38(12), 1107–1110. doi: 10.1130/G31145.1

MacLeod, K. G., Huber, B. T., & Isaza-Londoño, C. (2005). North Atlantic warming during global cooling at the end of the Cretaceous. Geology, 33, 437–440. https://doi.org/10.1130/G21466.1

Mahdi, A. Q., Al-Beyati, F. M., Al Tarif, A. M., Shendi, E. A. H., & Abdel-Fattah, M. I. (2019). Palynofacies and paleoenvironment investigation of the hauterivian–early aptian Ratawi and Zubair formations, Balad oilfield, Central Iraq. Tikrit Journal of Pure Science, 24(6), 74-80. http://dx.doi.org/10.25130/tjps.24.2019.111

Mahdi, A. Q., Abdel-Fattah, M. I., & Hamdan, H. A. (2022). An integrated geochemical analysis, basin modeling, and palynofacies analysis for characterizing mixed organic-rich carbonate and shale rocks in Mesopotamian Basin, Iraq: Insights for multisource rocks evaluation. Journal of Petroleum Science and Engineering, 216, 110832. http://dx.doi.org/10.1016/j.petrol.2022.110832

Mansour, A., Gentzis, T., Wagreich, M., Tahoun, S.S. & Elewa, A.M.T. (2020a). Short-term sea level changes of the Upper Cretaceous carbonates: Calibration between palynomorphs composition, inorganic geochemistry, and stable isotopes. Minerals, 10, 1099; doi:10.3390/min10121099

Mansour, A., Wagreich, M., Gentzis, T., Ocubalidet, S., Tahoun, S.S. & Elewa, A.M.T. (2020b). Depositional and organic carbon-controlled regimes during the Coniacian Santonian event: First results from the southern Tethys (Egypt). Marine and Petroleum Geology, 115, 10428. https://doi.org/10.1016/j.marpetgeo.2020.104285

Mansour, A., Gentzis, T., Ied, I.M. & Ahmed, M.S. (2022). Paleoenvironmental conditions and factors controlling organic carbon accumulation during the Jurassic–Early Cretaceous, Egypt: Organic and inorganic geochemical approach. Minerals, 12, 1213. https://doi.org/10.3390/min12101213

Mansour, A. & Wagreich, M. (2022). Earth system changes during the cooling greenhouse phase of the Late Cretaceous: Coniacian-Santonian OAE3 subevents and fundamental variations in organic carbon deposition. Earth- Science Reviews, 229, 104022. https://doi.org/10.1016/j.earscirev.2022.104022

Mansour, A. & Wagreich, M. (2023). An overview of the Cretaceous oceanic anoxic events (OAEs) in Egypt, southern Tethys. Geological Society London Special Publications, 545(1). DOI:10.1144/SP545-2023-104

März, C., Beckmann, B., Franke, C., Vogt, C., Wagner, T. & Kasten, S. (2009). Geochemical environment of the Coniacian–Santonian western tropical Atlantic at Demerara Rise. Palaeogeography Palaeoclimatology Palaeoecology, 273(3-4), 286-301. https://doi.org/10.1016/j.palaeo.2008.05.004

Mohammed, I.Q., Farouk, S., Mousa, A., Lawa, F.A., 2022. Lithofacies types, mineralogical assemblages and depositional model of the Maastrichtian–Danian successions in the Western Desert of Iraq and eastern Jordan. Journal of African Earth Sciences, 186, 104397. https://doi.org/10.1016/j.jafrearsci.2021.104397

Munier, T., Riquier, L., Révillon, S., Brumsack, H-J, Hasler, C., Boudouma, O. & François, B. (2023). Climatic and weathering conditions in southern high latitudes during the Turonian-Santonian interval: New insights from IODP Site U1512 (Bight Basin, Southern Australia). Palaeogeography Palaeoclimatology Palaeoecology, 613, 111413 (18p.) https://doi.org/10.1016/j.palaeo.2023.111413

O'Brien, C. L., Robinson, S. A., Pancost, R. D., Sinninghe Damsté, J. S., Schoulten, S., Lunt & D. J. (2017). Cretaceous sea-surface temperature evolution: Constraints from TEX_{86} and planktonic foraminiferal oxygen isotopes. Earth-Science Reviews, 172, 224–247. https://doi. org/10.1016/j.earscirev.2017.07.012

Ozyurt, M., Kirmaci, M. Z., Al-Aasm, I., Hollis, C., Tasli, K. & Kandemir, R. (2020). REE characteristics of Lower Cretaceous limestone succession in Gümüşhane, NE Turkey: Implications for ocean paleoredox conditions and diagenetic alteration. Minerals,10 (8) 683. https://doi.org/10.3390/min10080683

Petrizzo, M.R., Berrocoso, A.J., Falzoni, F. & Huber, B. (2017). The Coniacian-Santonian sedimentary record in southern Tanzania (Ruvuma Basin, East Africa): Planktonic foraminiferal evolutionary, geochemical and palaeoceanographic patterns. Sedimentology, 64(1). DOI:10.1111/sed.12331

Petrizzo, M.R., MacLeod, K.G., Watkins, D.K., Wolfgring, E. & Huber, B.T. (2022). Late Cretaceous paleoceanographic evolution and the onset of cooling in the Santonian at southern high latitudes (IODP Site U1513, SE Indian Ocean). AGU Advancing *Earth and Space Science, 37(1), 1-38*. https://doi.org/10.1029/2021PA004353

Peucker-Ehrenbrink, B. & Ravizza, G. (2000). The marine osmium isotope record. Terra Nova, 12(5):205 – 219. http://dx.doi.org/10.1046/j.1365-3121.2000.00295.x

Phelps, R.M., Kerans, C., Da-Gama, R., Jeremiah, J., Hull, D. & Loucks, R.L. (2015). Response and recovery of the Comanche carbonate platform surrounding multiple Cretaceous oceanic anoxic events, northern Gulf of Mexico. Cretaceous Research, 54, 117-144. https://doi.org/10.1016/j.cretres.2014.09.002

Pohl, A., Donnadieu, Y., Godderis, Y., Lanteaume, C., Hairabian, A., Frau, C., Michel, J., Laugie, M., Reijmer, J.J.G. & Scotese, R. (2020). Carbonate platform production during the Cretaceous. GSA Bulletin, 132 (11-12): 2606–2610.https://doi.org/10.1130/B35680.1

Remin, Z. (2004). Biostratigraphy of the Santonian in the SW margin of the Holy Cross Mountains near Lipnik, a potential reference section for extra -Carpathian Poland. Acta Geologica Polonica, 54(4) 587-596.

Sachse, V.F., Littke, R., Jabour, H., Schümann, T. & Kluth, O. (2012). Late Cretaceous (Late Turonian, Coniacian and Santonian) petroleum source rocks as part of an OAE, Tarfaya Basin, Morocco. Marine and Petroleum Geology, 29, 35-49. https://doi.org/10.1016/j.marpetgeo.2011.08.014

Sadooni, F.N. (2004). Stratigraphy, depositional setting and reservoir characteristics of Turonian - Campanian carbonates in Central Iraq. Journal of Petroleum Geology, 27 (4), 357- 371. DOI:10.1111/j.1747-5457.2004.tb00063.x

Schlanger, S. O. & Jenkyns, H. C. (1976). Cretaceous Oceanic Anoxic Events: Causes and consequences. Geologie en Mijnbouw, 55(3), 179- 184.

Smith, B. P., Kerans, C. & Fischer, W. W. (2021). A redox-based model for carbonate platform drowning and Ocean Anoxic Events. Geophysical Research Letters, 48, e2021GL093048. https://doi.org/10.1029/2021GL093048

Steuber, T., Loser, H., Mutterlose, J. & Parente, M. (2023). Biogeodynamics of Cretaceous marine carbonate production. Earth-Science Reviews, 238, 104341. https://doi.org/10.1016/j.earscirev.2023.104341

Sun, W., Li, C-Y., Hao, X-L., Ling, M.X., Ireland, T.R., Ding, X. & Fan, W.M. (2016). Oceanic anoxic events, subduction style and molybdenum mineralization. Solid Earth Sciences, 1(2), 64-73. https://doi.org/10.1016/j.sesci.2015.11.001

Su, N., Yang, S., Guo, Y., Yue, W., Wang, X., Yin P., & Huang, X. (2017). Revisit of rare earth element fractionation during chemical weathering and river sediment transport. Geochemistry, Geophysics, Geosystems, 18(3) DOI:10.1002/2016GC006659

Taylor, S. R. & McLennan, S. H. (1985). The geochemical evolution of the continental crust. Review Geophysics, 33, 241-265. https://doi.org/10.1029/95RG00262

Tessin, A., Hendy, I., Sheldon, N. & Sageman, B. (2015). Redox-controlled preservation of organic matter during "OAE 3" within the Western Interior Seaway. Paleoceanography, 30, 702–717, doi:10.1002/2014PA002729.

Tostevin, R. (2021). Cerium Anomalies and Paleoredox. (Elements in Geochemical Tracers in Earth Systems Science). Cambridge University Press, Cambridge. https://doi.org/10.1017/9781108847223

Tsikos, H. Jenkyns, H.C., Walsworth-Bell, B., Petrizzo, M.R., Forster, A., Kolonic, S., Erba, E., Silva, I.P., Baas, M., Wagner, T. & Sinninghe-Damste, J.S. (2004). Carbon-isotope stratigraphy recorded by the Cenomanian–Turonian oceanic anoxic event: Correlation and implications based on three key localities. Journal of Geological Society, 161, 711–719. DOI:10.1144/0016-7649Er161-4

Wagreich, M. (2009). Coniacian–Santonian Oceanic red beds and their link to Oceanic Anoxic Event 3. in Cretaceous Ocean Redbeds: Stratigraphy, Composition, Origins, and Paleoceanographic and Paleoclimatic Significance (eds. Hu, X., Wang, C., Scott, R. W., Wagreich, M. & Jansa, L.) 235–242 (SEPM (Society for Sedimentary Geology). https://doi.org/10.2110/sepmsp.091.

Wagreich, M. (2012). 'OAE 3'—regional Atlantic organic carbon burial during the Coniacian–Santonian. *Climate of the Past*, 8, 1447–1455. https://doi.org/10.5194/cp-8-1447-2012

Wagreich, M. & Mansour, A. (2022). The Coniacian-Santonian Oceanic Anoxic Event OAE3 - global correlation of subevents. EGU22, the 24th EGU General Assembly, held 23-27 May, 2022 in Vienna, Austria. https://ui.adsabs.harvard.edu/link_gateway/2022EGUGA.2411382W/doi:10.5194/egusphere-egu22-11382

Wang, T., Ramezani, J., Wang, C., Wu, H., He, H. & Bowring, S.A. (2016). High-precision U–Pb 755 geochronologic constraints on the Late Cretaceous terrestrial cyclostratigraphy and 756 geomagnetic polarity from the Songliao Basin, Northeast China. *Earth* and *Planetary* Science *Letters,* 446, 37-44. DOI:10.1016/j.epsl.2016.04.007

Wendler, I., Wendler, J., Gräfe, K.-U., Lehmann, J. & Willems, H. (2009). Turonian to Santonian carbon isotope data from the Tethys Himalaya, southern Tibet. Cretaceous Research, 30(4), 961-979. https://doi.org/10.1016/j.cretres.2009.02.010

Wendler, I. (2013). A critical evaluation of carbon isotope stratigraphy and biostratigraphic implications for Late Cretaceous global correlation. Earth-Science Reviews, 126, 116–146. https://doi.org/10.1016/j.earscirev.2013.08.003

Wu, H., Zhang, S., Jiang, G., Hinnov, L., Yang, T., Li, H., Wan, X. & Wang, C. (2013). Astrochronology of the 762 Early Turonian-Early Campanian terrestrial succession in the Songliao Basin, northeastern China and its implication for long-period behavior of the Solar System. Palaeogeography Palaeoclimatology Palaeoecology, 385, 55-70. DOI:10.1016/j.palaeo.2012.09.004

Xu, Y., Li, D., Gao, Y., Li, M., Sun, L., Zhang, S., Wang, C. & Shen, Y. (2023). Multiple S-isotopic evidence for seawater incursions during the deposition of the upper Cretaceous source rocks in the Songliao Basin, northeastern China. Chemical Geology, 642, 121790. https://doi.org/10.1016/j.chemgeo.2023.121790

Yilmaz, I.O., Cook, T.D., Hosgor, I. & Wagreich, M. (2018). The upper Coniacian to upper Santonian drowned Arabian carbonate platform, the Mardin-Mazidag area, SE Turkey: Sedimentological, stratigraphic, and ichthyofaunal records. Cretaceous Research, 84, 153-167. https://doi.org/10.1016/j.cretres.2017.09.012

Zhao, M. & Zheng, Y-F. (2014). Marine carbonate records of terrigenous input into Paleotethyan seawater: Geochemical constraints from Carboniferous limestones. Geochimica et Cosmochimica Acta, 141:508–531. DOI:10.1016/j.gca.2014.07.001

Zhang, K. & Shields, G.A. (2022). Sedimentary Ce anomalies: Secular change and implications for paleoenvironmental evolution. Earth-Science Reviews, 229, 104015. https://doi.org/10.1016/j.earscirev.2022.104015